July 2002 • NREL/MP-540-32709

Milestone Report

Enhancements to NREL System Analysis Tools to Improve Auxiliary Load Modeling and Air Conditioner Modeling for Heavy Vehicles

Milestone Completion Report

Michael O'Keefe
Terry Hendricks
Jason Lustbader
Aaron Brooker

National Renewable Energy Laboratory
Golden, Colorado

Prepared for the DOE
Office of Energy Efficiency and Renewable Energy
In fulfillment of July 2002 Fuels Utilization Milestone 3.2.1

National Renewable Energy Laboratory

1617 Cole Boulevard
Golden, Colorado 80401-3393

NREL is a U.S. Department of Energy Laboratory
Operated by Midwest Research Institute • Battelle • Bechtel

Contract No. DE-AC36-99-GO10337

Enhancements to NREL System Analysis Tools to Improve Auxiliary Load Modeling and Air Conditioner Modeling for Heavy Vehicles

Michael O'Keefe
Terry Hendricks
Jason Lustbader
Aaron Brooker

Center for Transportation Technologies and Systems
National Renewable Energy Laboratory
Golden, Colorado

Prepared under FWP FU23 in fulfillment of the milestone/deliverable entitled
"Report documenting enhancements to NREL systems analysis tools (ADVISOR) to improve auxiliary load modeling and air conditioner modeling for heavy vehicles"

For the
U.S. Department of Energy
Office of Energy Efficiency and Renewable Energy

National Renewable Energy Laboratory
1617 Cole Boulevard
Golden, Colorado 80401-3393
A national laboratory of the U.S. Department of Energy
Managed by the Midwest Research Institute, Battelle, and Bechtel

NOTICE

Available electronically at http://www.osti.gov/bridge

Available for a processing fee to U.S. Department of Energy and its contractors, in paper, from:

U.S. Department of Energy
Office of Scientific and Technical Information
P.O. Box 62
Oak Ridge, TN 37831-0062
phone: 865.576.8401
fax: 865.576.5728
email: reports@adonis.osti.gov

Available for sale to the public, in paper, from:

U.S. Department of Commerce
National Technical Information Service
5285 Port Royal Road
Springfield, VA 22161
phone: 800.553.6847
fax: 703.605.6900
email: orders@ntis.fedworld.gov
online ordering: http://www.ntis.gov/ordering.htm

Printed on paper containing at least 50% wastepaper, including 20% postconsumer waste

Executive Summary

This paper presents an overview of enhancements to NREL's system analysis tools for modeling of heavy vehicle auxiliary loads. Auxiliary load applications for several different models and methods are presented. These include ADVISOR (ADvanced VehIcle SimulatOR) auxiliary load models, model co-simulations with Saber and SINDA/FLUINT, thermoelectric models, VSOLE (Vehicle Solar Load Estimator), and WAVE.

ADVISOR auxiliary load models offer speed-dependent mechanical and time-variable electrical load modeling. Saber co-simulation with ADVISOR enables assessment of the fuel economy impact of detailed electrical models. SINDA/FLUINT co-simulation with ADVISOR allows vehicle air conditioning (A/C) systems and fuel economy impact to be modeled in detail.

Thermoelectric models assess the possible energy that can be recovered from waste heat. VSOLE assesses the solar loading on a vehicle, which is important for cabin thermal analysis. WAVE is an engine model capable of generating key thermal information for ADVISOR and other tools.

Several of these modeling enhancements have played key roles in completing technical analyses. Logical next steps with these models include validation and application with industry partners.

Table of Contents

1 Introduction 7
2 Overview of Enhancements 7
3 Details on Enhancements 8
3.1 ADVISOR Auxiliary Load Models 8
3.1.1 Speed-dependent Auxiliary Loads 10
3.1.2 Time-variable Electrical Loads 18
3.2 Saber Co-simulation of Electrical Loads 21
3.3 SINDA/FLUINT Co-simulation 24
3.4 Thermoelectric Models 33
3.5 Vehicle Solar Load Estimator 43
3.6 WAVE 43
4 Next Steps 47
4.1 ADVISOR Auxiliary Load Model 47
4.2 Saber Co-simulation 48
4.3 SINDA/FLUINT Co-simulation Model 48
4.4 Thermoelectric Models 48
4.5 VSOLE and Cabin Thermal Modeling 48
4.6 WAVE 48
5 Conclusion 49
6 Bibliography 49

Table of Figures

Figure 1 CSHVR Drive Cycle 9
Figure 2 Constant 65-mph Drive Cycle 9
Figure 3 WVU Interstate Drive Cycle 10
Figure 4 Air Condition Compressor Power Consumption vs. Engine Shaft Speed..... 11
Figure 5 Engine Fan Power Consumption vs. Engine Shaft Speed 11
Figure 6 Power Steering Pump Power Consumption vs. Engine Shaft Speed 11
Figure 7 Air Brake Compressor Power Consumption vs. Engine Shaft Speed 11
Figure 8 Power Consumption Profile for an Active Air Brake Compressor over CSHVR Drive Cycle 12
Figure 9 Power Consumption Profile for an Inactive Air Brake Compressor over CSHVR Drive Cycle 12
Figure 10 Fuel Savings Predicted over CSHVR when Mechanical Loads Removed for Five Different Engines 13
Figure 11 Fuel Savings Predicted over Constant 65 mph when Mechanical Loads Removed 13
Figure 12 Constant vs. Speed-Dependent Auxiliary Load over CSHVR 14
Figure 13 Fuel Economy Difference Between Constant (red-bottom) and Variable Speed (yellow-top) Mechanical Loads 15
Figure 14 Air Conditioning Transient Load for First 360 sec of Drive Cycle 16
Figure 15 Variable Load vs. Constant Set at Average of Variable Load for Tractor-trailer Model over CSHVR..... 16
Figure 16 Miles Per Gallon over CSHVR for Constant vs. Variable Mechanical Load Model Run 17
Figure 17 Gallons of Fuel Used over CSHVR for Constant vs. Variable Mechanical Load Model Run 17
Figure 18 Difference in Predicted Fuel Use for Constant vs. Variable Electrical Loads . 19
Figure 19 Auxiliary Load on Engine vs. Time with a Constant 60% Efficient Alternator 20
Figure 20 Auxiliary Load on Engine vs. Time with a Variable-efficiency Alternator..... 20
Figure 21 Saber Schematic of Conventional Vehicle 14-V Electrical System (Saber-ADVISOR Co-simulation)..... 22
Figure 22 Predicted Fuel Economy Using Three Different Auxiliary Load Models over CSHVR Drive Cycle..... 22
Figure 23 Starting-lighting-ignition Battery SOC History during CSHVR..... 23
Figure 24 Current History of Power Bus over CSHVR..... 24
Figure 25 SINDA/FLUINT Transient A/C Loop for Class 6 Truck Cabin 25
Figure 26 The SC03 Drive Cycle..... 25
Figure 27 Predicted Cabin Temperature vs. Time over the SC03 Drive Cycle..... 26
Figure 28 Predicted Air Temperatures into and out of the Evaporator over the SC03 Drive Cycle 27
Figure 29 A/C Compressor Power over the SC03 Drive Cycle..... 27
Figure 30 Predicted High and Low Pressures along the A/C Loop vs. Time over the SC03 Drive Cycle 28
Figure 31 A/C Loop Pressures on a Semi-log Scale vs. Time over SC03 Drive Cycle ... 28

Figure 32 Enthalpy at Various Points around the A/C Loop vs. Time 29
Figure 33 Temperatures at Various Points around the A/C Loop vs. Time 29
Figure 34 Quality at Various Points around the A/C Loop vs. Time 30
Figure 35 Quality at Various Points through the Condenser vs. Time 30
Figure 36 Quality at Various Points through the Evaporator vs. Time 31
Figure 37 Quality by Length through the Evaporator at Various Times along the SC03 Drive Cycle 31
Figure 38 Pressure-enthalpy Diagram Depicting the Regions of Operation of Four Points in the A/C System Superimposed over the R-134a Vapor Dome 32
Figure 39 Fuel Economy Predicted by ADVISOR-SINDA/FLUINT Co-simulations with Designated Starting Conditions 32
Figure 40 Cabin Temperature vs. Time for the ADVISOR-SINDA/FLUINT Co-simulation with Two Starting Temperatures (123 F and 131 F) and Two Drive Cycles (CSHVR and SC03) 33
Figure 41 Thermoelectric Element 34
Figure 42 Thermoelectric Device with Multi-material Legs 34
Figure 43 *p*-type Material ZT vs. Temperature Characteristics 35
Figure 44 *n*-type Material ZT vs. Temperature Characteristics 35
Figure 45 Predicted Electrical Power Available from Skutterudite-Bi_2Te_3 and $CoSb_3$-Bi_2Te_3 (NASA-Jet Propulsion Laboratory, Pasadena, CA) Thermoelectric Material Operating at the Given Hot- and Cold-side Temperatures and Exhaust Mass Flow Rates 36
Figure 46 Required Cold-side Mass Flow Rates from Skutterudite-Bi_2Te_3 and $CoSb_3$-Bi_2Te_3 (NASA-Jet Propulsion Laboratory, Pasadena, CA) Thermoelectric Material Operating at Peak Power at the Given Hot- and Cold-side Temperatures and Exhaust Mass Flow Rates 37
Figure 47 Predicted Electrical Power Available from a Skutterudite-Zn_4Sb_3-Bi_2Te_3 and $CoSb_3$-Bi_2Te_3 Thermoelectric Material Operating at the Given Hot- and Cold-side Temperatures and Exhaust Mass Flow Rates 38
Figure 48 Required Cold-side Mass Flow Rates from a Skutterudite-Zn_4Sb_3-Bi_2Te_3 and $CoSb_3$-Bi_2Te_3 Thermoelectric Material Operating at Peak Power at the Given Hot- and Cold-side Temperatures and Exhaust Mass Flow Rates 38
Figure 49 Efficiency vs. Maximum Electrical Power Output for Skutterudite-Bi_2Te_3 and $CoSb_3$-Bi_2Te_3 Thermoelectric Device in WAVE 10-L CI Engine 39
Figure 50 Predicted Electrical Power Available from TAGS-Bi_2Te_3 and 2NPbTe-Bi_2Te_3 (Hi-Z Technology Inc., San Diego, CA) Thermoelectric Material Operating at the Given Hot- and Cold-side Temperatures and Exhaust Mass Flow Rates (Water Cooled) 40
Figure 51 Required Cold-side Mass Flow Rates from TAGS-Bi_2Te_3 and 2NPbTe-Bi_2Te_3 (Hi-Z Technology Inc., San Diego, CA) Thermoelectric Material Operating at Peak Power at the Given Hot- and Cold-side Temperatures and Exhaust Mass Flow Rates (Water Cooled) 40
Figure 52 Efficiency vs. Maximum Electrical Power Output for TAGS-Bi_2Te_3 and 2NPbTe-Bi_2Te_3 Thermoelectric Device in WAVE 10-L CI Engine (Water Cooled) 41

Figure 53 Cold-side Mass Flow Rate Requirements for a Post-compressor Thermoelectric Device 42
Figure 54 Peak Power by Heat Exchanger Resistance for a Post-compressor Thermoelectric Device 42
Figure 55 Full-load WAVE-mapped Engine Power vs. Tested Power 43
Figure 56 Full-load WAVE-mapped Engine Torque vs. Tested Torque 43
Figure 57 Full-load WAVE-mapped Engine Brake-specific Fuel Consumption (BSFC) vs. Tested BSFC 44
Figure 58 Full-load WAVE-mapped Engine Fuel Rate vs. Tested Fuel Rate 44
Figure 59 Partial-load WAVE-mapped Engine BSFC vs. Tested BSFC 44
Figure 60 Partial-load WAVE-mapped Engine Fuel Rate vs. Tested Fuel Rate 44
Figure 61 WAVE-generated Engine Map Showing Efficiency by Torque and Speed (Based on Navistar T444) 45
Figure 62 Efficiency Map Generated Using Base Data 45
Figure 63 Difference Map Showing Difference Between WAVE-predicted Efficiency and an Engine Map Based on Test Data 46
Figure 64 Engine Exhaust Temperature by Shaft Torque and Speed as Predicted by WAVE Navistar T444 Model 47
Figure 65 Engine Exhaust Mass Flow Rate as Predicted by WAVE Navistar T444 Model 47

Table of Tables

Table 1 Tractor-trailer Model Specifications (Based on 21st Century Truck Roadmap Model) 52
Table 2 Baseline Tractor-trailer Model in ADVISOR (80,000 lb GVW) 52
Table 3 Tractor-trailer Model with Speed-dependent Mechanical Loads in ADVISOR (80,000 lb GVW, variable SAEJ1343—local haul, 1466.9 W electrical load on alternator) 52
Table 4 Baseline Constant Electrical/Mechanical Auxiliary Load Tractor-trailer Model in ADVISOR—60% efficient alternator (80,000 lb GVW) 52
Table 5 Time-variable Electrical Loads for Tractor-trailer Model in ADVISOR (80,000 lb GVW)—60% efficient alternator 53
Table 6 Time-variable Electrical Loads for Tractor-trailer Model in ADVISOR (80,000 lb GVW)—Variable Efficiency Alternator with Time-variable Electrical Loads and Fixed Constant Electrical Loads 53
Table 7 Saber Co-simulation with Tractor-trailer Model in ADVISOR (80,000 lb GVW) 53
Table 8 WAVE-predicted Efficiency vs. 13-mode OICA* Cycle Test Data 54

1 Introduction

Auxiliary loads are not directly linked to vehicle propulsion but they use a significant amount of fuel, especially in heavy vehicles. The demand for vehicle auxiliary power is growing.

Traditionally, energy use from auxiliary loads has not received much attention. Auxiliary devices are designed to be durable and dependable but not necessarily efficient. In addition, conventional mechanically driven devices include minimal, if any, control. Thus, auxiliary devices tend to be oversized and non-optimized for the vast majority of operating conditions.

Significant energy savings can be realized by reducing the inefficiencies of traditional auxiliary loads. Implementation of an efficient energy management strategy is key to achieving energy savings. NREL is exploring and quantifying the energy savings possible with an auxiliary energy management strategy. Enhancements in vehicle system analysis tools are necessary to conduct this analysis.

Several enhancements to NREL's system analysis tools for studying auxiliary systems have been made over the past fiscal year. Most improvements are connected with ADVISOR, NREL's vehicle system analysis tool. Other simulation codes have been used as well. These include the multi-domain simulation software Saber (Synopsys/Avant!) and a similar code, SIMPLORER (Ansoft), for electrical simulation. The engine simulation software WAVE (Ricardo) and thermal-fluid software SINDA/FLUINT (C&R Technologies) have been used as well.

Most tools described in this paper are included with or documented for use with ADVISOR 2002. ADVISOR 2002 is an open-source code that is freely available to the public (ADVISOR 2002).

This paper gives an overview of enhancements made to NREL's system analysis tools related to auxiliary loads and A/C modeling. This overview is focused on heavy-duty vehicle applications, but these tools can be readily applied to other vehicle platforms.

The first section of this paper gives a general overview of enhancements. Next, these enhancements are discussed in detail with applications. Instruction on using the models is not provided, but references are given where possible. Finally, notes on future directions for these tools are provided.

2 Overview of Enhancements

ADVISOR is one of NREL's main vehicle system analysis tools. Many of the enhancements made to enable auxiliary load modeling involve ADVISOR.

ADVISOR is open-source, publicly available vehicle simulation software developed at NREL (Markel *et al.* 2002, Wipke *et al.* 1999, ADVISOR 2002). ADVISOR simulates conventional and advanced vehicles. Advanced vehicles include internal-combustion engine hybrids, fuel cell vehicles, and alternative fuel vehicles.

Advances in the auxiliary load model in ADVISOR have enabled new areas of research. For example, ADVISOR has been used for transient A/C optimization (with SINDA/FLUINT; Cullimore and Hendricks 2001, Hendricks 2001a, Hendricks 2001b)

and auxiliary energy quantification (Hendricks and O'Keefe 2002). ADVISOR has also been used in conjunction with Saber to examine electrical loads (MacBain and Conover 2000, MacBain and Conover 2001, MacBain and Conover 2001a, MacBain *et al.* 2001).

Below is a list of auxiliary and A/C-related modeling enhancements to NREL's system analysis tools:

- Shaft speed–dependent mechanical auxiliary load modeling in ADVISOR
- Time-variable electrical auxiliary load modeling in ADVISOR
- Vehicle electrical system simulation using Saber in conjunction with ADVISOR
- Transient A/C analysis with SINDA/FLUINT: standalone and co-simulation with ADVISOR
- Thermoelectric device modeling
- VSOLE for estimation of solar load on vehicles
- Engine modeling using WAVE

3 Details on Enhancements

3.1 ADVISOR Auxiliary Load Models

In earlier versions of ADVISOR (versions 3.1 and earlier), auxiliary loads were modeled as constant power loads. Time-variable electrical loads were introduced with the release of ADVISOR 3.2. In ADVISOR 2002, speed-dependent mechanical loads and the ability to perform co-simulations with common auxiliary load modeling tools were added. The co-simulation set-ups include Saber, SIMPLORER, and SINDA/FLUINT. More information about using ADVISOR and running ADVISOR-related models is available on the Web (ADVISOR 2002).

To contrast the different auxiliary load models in ADVISOR, an example vehicle is used throughout the following sections. This vehicle is the tractor-trailer used in the "Technology Roadmap for the 21st Century Truck Program: A Government-Industry Partnership," December 2000 (21CT 2000).

Three different drive cycles are used to evaluate the model. The first is a constant 65-mph drive cycle. The next is the CSHVR (city suburban heavy vehicle route) developed by West Virginia University (WVU) (Clark *et al.* 1999, LeTavec *et al.* 2000). The last is the WVU Interstate drive cycle. These drive cycles are depicted in Figure 1, Figure 2, and Figure 3.

The baseline vehicle's energy use and specifications are given in Table 1 and Table 2, Appendix A. The baseline vehicle achieves 6.6 mpg at a constant 65 mph.

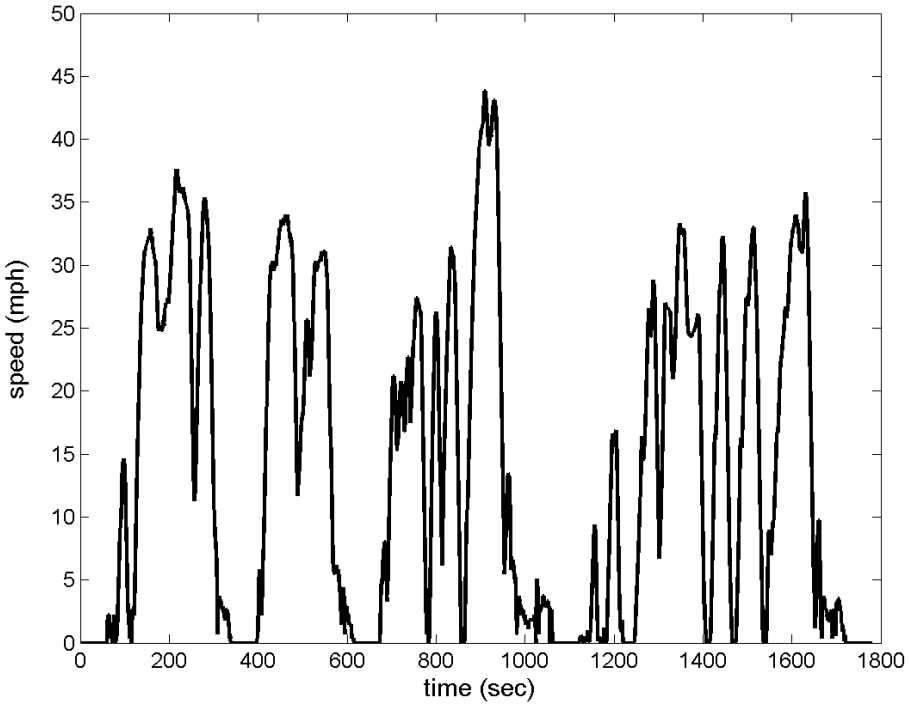

Figure 1 CSHVR Drive Cycle

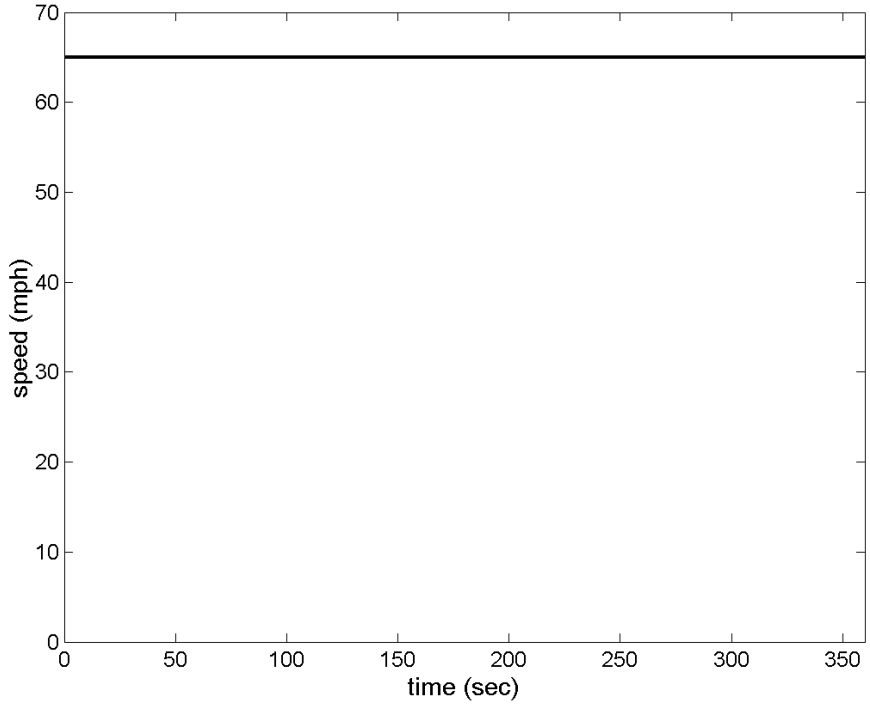

Figure 2 Constant 65-mph Drive Cycle

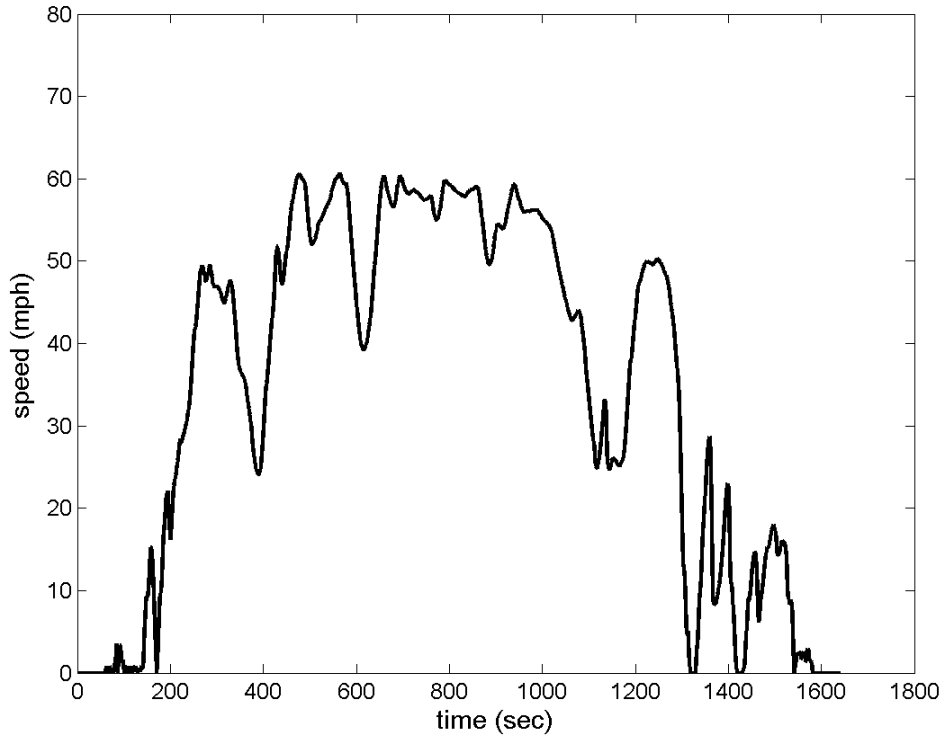

Figure 3 WVU Interstate Drive Cycle

3.1.1 Speed-dependent Auxiliary Loads

Conventional mechanical auxiliary loads are belt driven and powered by the engine. Alternatively, they may be powered through a power takeoff from the transmission. The power consumed by conventional auxiliary devices varies by shaft speed and device loading. Device loading can be thought of as on/off, loaded/unloaded, declutched/engaged, or high/low/off. SAE 2000 discusses typical heavy vehicle auxiliary duty cycles.

The speed-dependent auxiliary load model in ADVISOR simulates auxiliary power used by conventional mechanical auxiliary devices throughout a drive cycle. The model uses a lookup table based on speed and load (Hnatczuk *et al.* 2000). Typical speed-load curves are given for four auxiliary devices in Figure 4, Figure 5, Figure 6, and Figure 7.

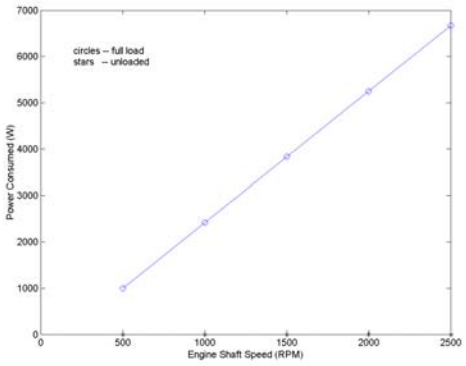

Figure 4 Air Condition Compressor Power Consumption vs. Engine Shaft Speed

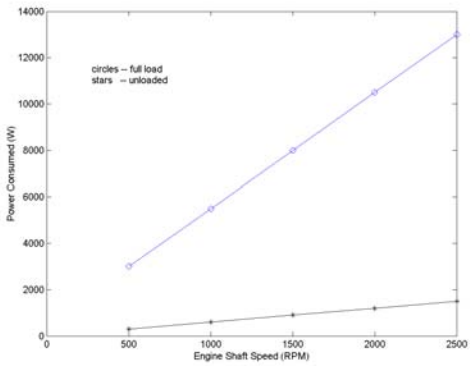

Figure 6 Power Steering Pump Power Consumption vs. Engine Shaft Speed

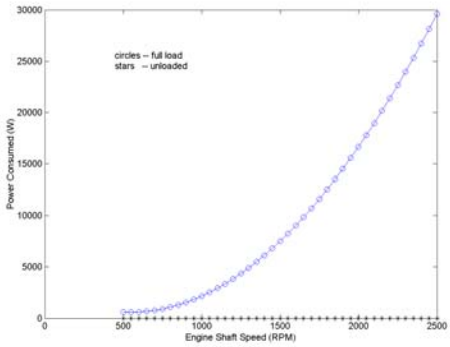

Figure 5 Engine Fan Power Consumption vs. Engine Shaft Speed

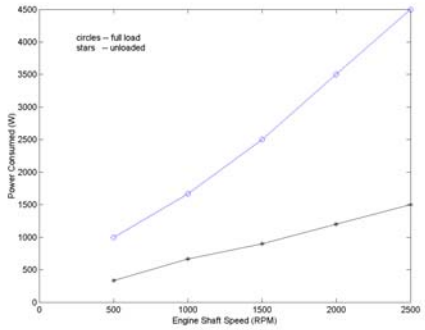

Figure 7 Air Brake Compressor Power Consumption vs. Engine Shaft Speed

There are two power consumption curves on each figure. The high curve (blue circles) represents power consumed when the device is fully loaded (i.e., on at its maximum setting). The low curve (black stars) represents power consumed while unloaded or "off." For the A/C compressor and engine fan, the device is modeled as unclutched when not loaded. Thus, energy is not consumed when the device is unloaded. However, for the power steering pump in Figure 6 and air brake compressor in Figure 7, this is not the case. These devices are drawing power from the engine even when not generating useful work.

The speed-dependent load model in ADVISOR quantifies wasted energy from components "dragging" on the engine. The power profile of an air brake compressor while loaded and unloaded is shown in Figure 8 and Figure 9.

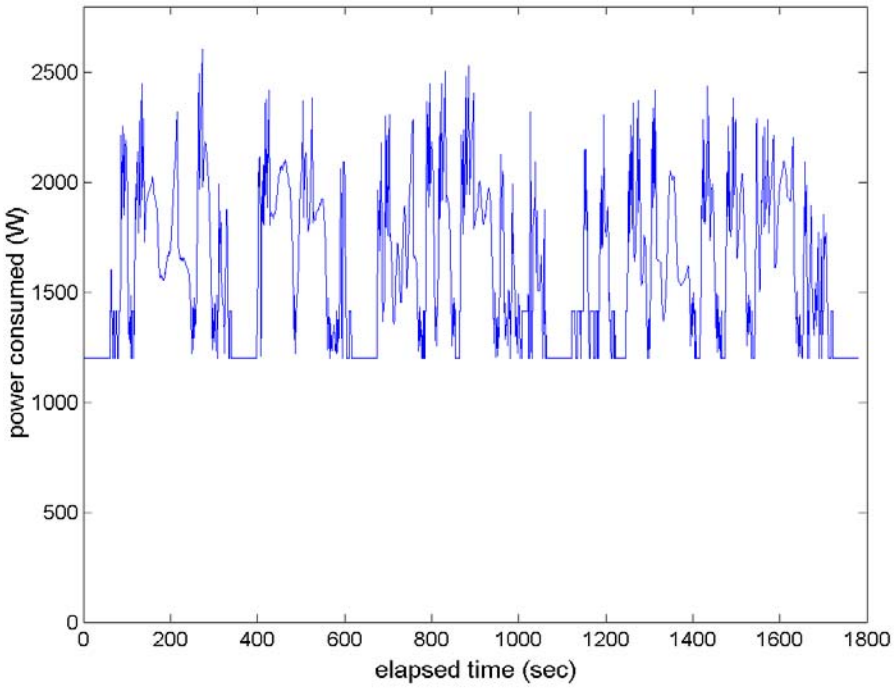

Figure 8 Power Consumption Profile for an Active Air Brake Compressor over CSHVR Drive Cycle

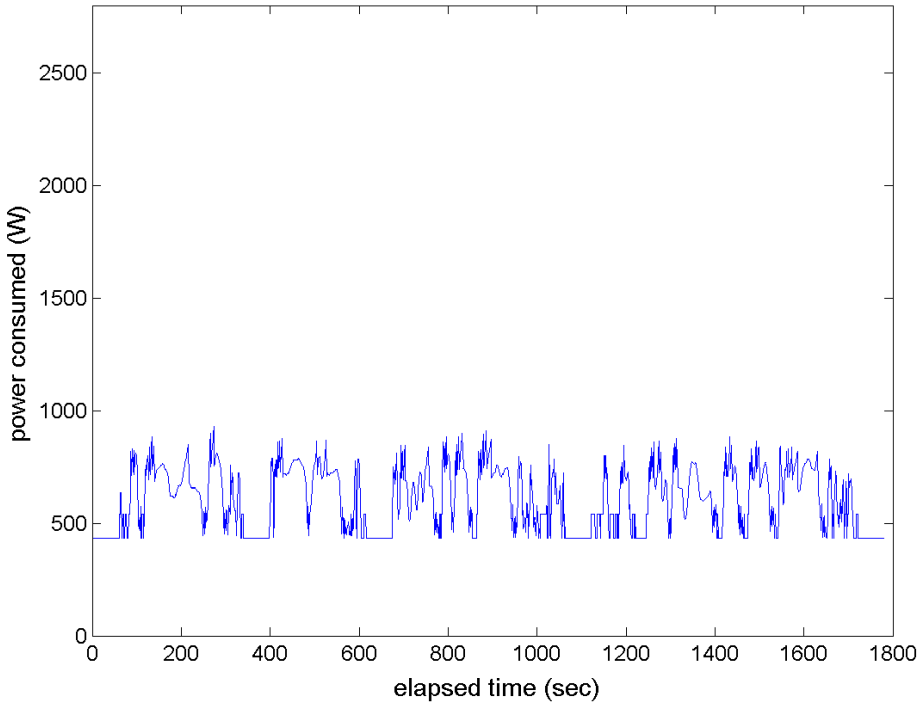

Figure 9 Power Consumption Profile for an Inactive Air Brake Compressor over CSHVR Drive Cycle

The air brake compressor uses 2864 kJ of energy over the CSHVR when actively compressing air. When not loaded, the compressor wastes 1084 kJ of energy over the CSHVR. This is about 1% of the total fuel energy used to drive the vehicle.

Fuel saved by removing conventional mechanical auxiliary loads from a heavy-duty engine was assessed using the speed-dependent auxiliary loads model (Figure 10 and Figure 11). This work contributed to DOE's Essential Power System Program (EPS 2001, Virden 2002).

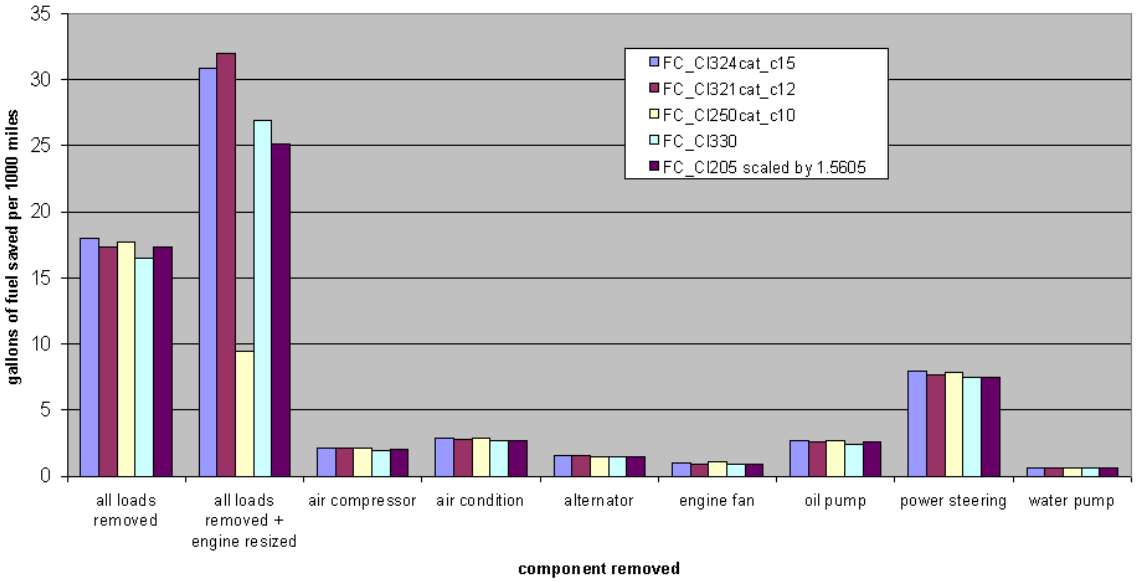

Figure 10 Fuel Savings Predicted over CSHVR when Mechanical Loads Removed for Five Different Engines

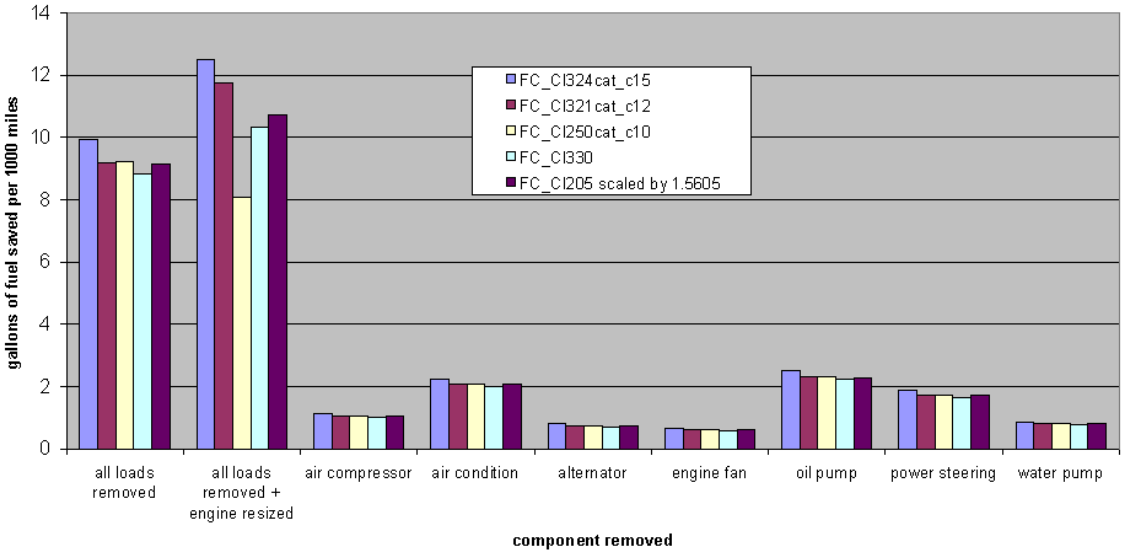

Figure 11 Fuel Savings Predicted over Constant 65 mph when Mechanical Loads Removed

Figure 10 and Figure 11 show fuel savings per distance traveled over the given drive cycles. Five different heavy-duty engines were used in the simulation. The advantages of

load removal and engine downsizing are illustrated in these figures. More information on this analysis is available (Hendricks and O'Keefe 2002).

The results of the 21st Century Truck tractor-trailer model run using speed-dependent, variable mechanical loads are presented next. The variable mechanical loads are set so the total auxiliary energy is equal to a 15-kW constant auxiliary baseline at 65 mph (Figure 2). This can be done because variable mechanical loads change with engine speed. The engine speed is constant when vehicle speed is constant. Therefore, the speed-variable load can be made equal to a constant load for the cycle duration.

Speed-dependent mechanical loads vary according to representative speed-load charts (such as Figure 4, Figure 5, Figure 6, and Figure 7). The auxiliary duty cycle is the time profile of when an auxiliary device is loaded or unloaded (i.e., "on" or "off"). The auxiliary duty cycle is held constant for this example.

Table 3 of Appendix A shows results from the speed-dependent mechanical load model run. Figure 12 shows the auxiliary power profile versus time: the speed-dependent mechanical load profile over the CSHVR is represented by the blue line, and the baseline constant value is represented by the black line. The model results correspond to the CSHVR cycle (Figure 1). Note that the variable mechanical power varies over the CSHVR cycle because this cycle is not a constant speed cycle.

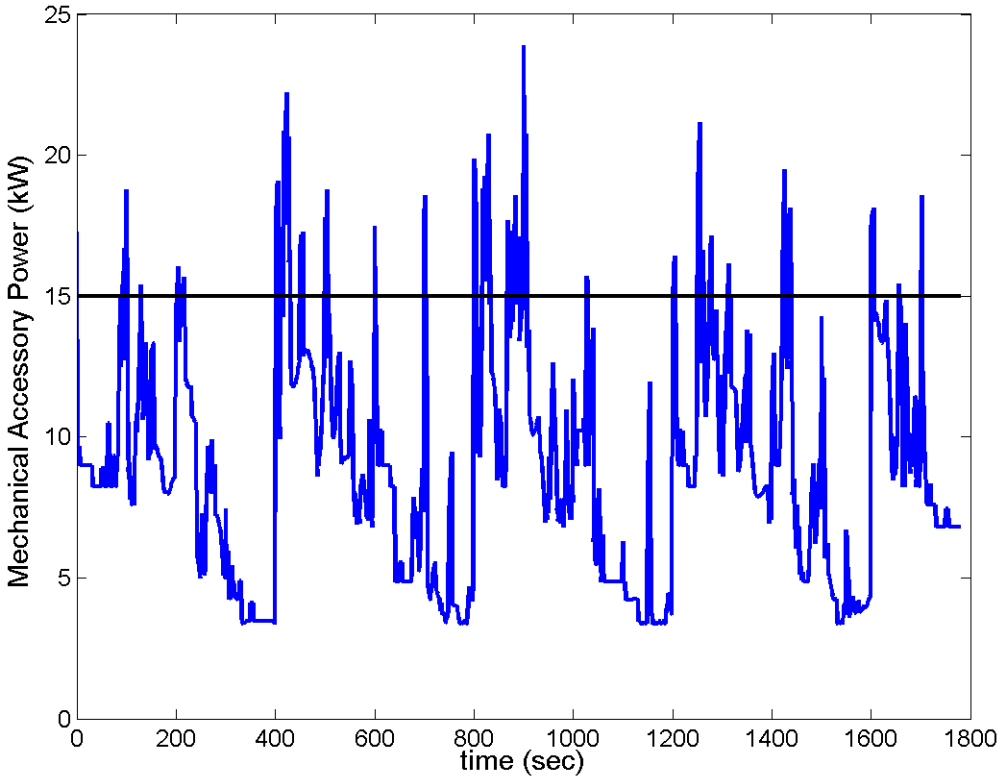

Figure 12 Constant vs. Speed-Dependent Auxiliary Load over CSHVR

On the CSHVR and Interstate cycles, the engine average speed is lower than the constant value at 65-mph. Because the power demanded by accessories is speed dependent,

auxiliary loads decrease as average engine speed decreases. This is shown by predicted fuel economy (Figure 13). Note in Figure 13 that fuel economy for the same drive cycle is better under variable auxiliary loads than constant loads.

Speed-dependent and constant auxiliary loads use the same energy for a vehicle at a constant 65 mph. However, lower engine speeds results in lower overall auxiliary load for the speed-dependent auxiliary load model. Thus, when the model runs under speed-dependent auxiliary loads, fuel economy is better. In contrast, the constant auxiliary load model always demands the same power—overestimating auxiliary loads in this case.

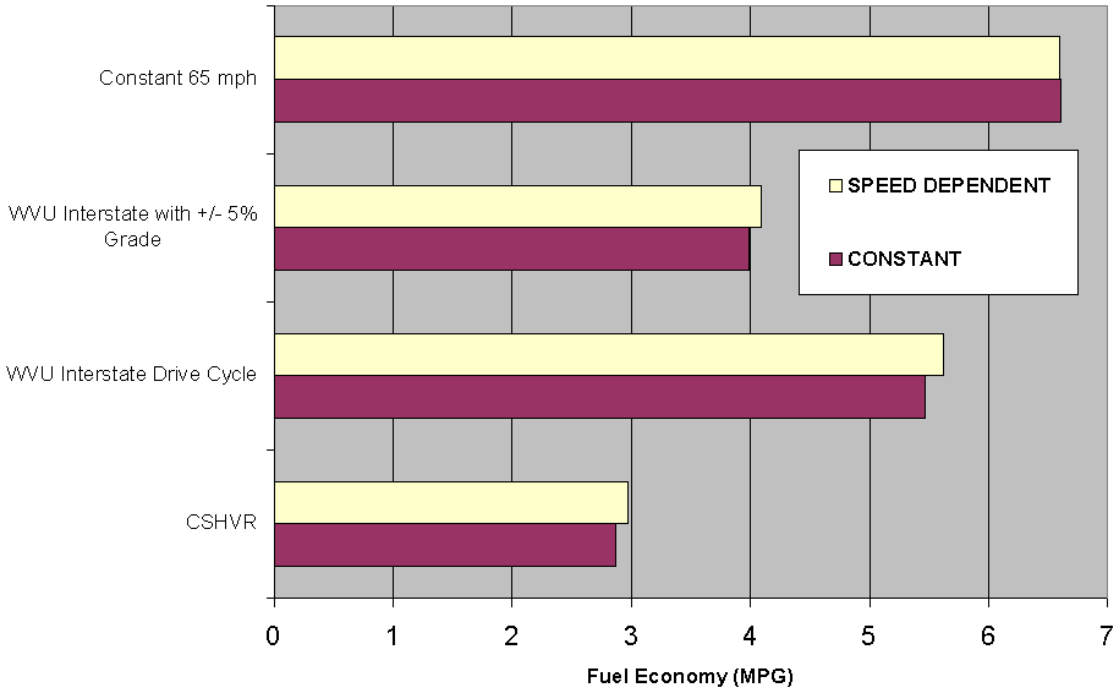

Figure 13 Fuel Economy Difference Between Constant (red-bottom) and Variable Speed (yellow-top) Mechanical Loads

Individual auxiliary devices can be examined in addition to total load. Figure 14 shows the power profile versus time for the A/C compressor over several drive cycles. The device is evenly cycled on, off, on, off.

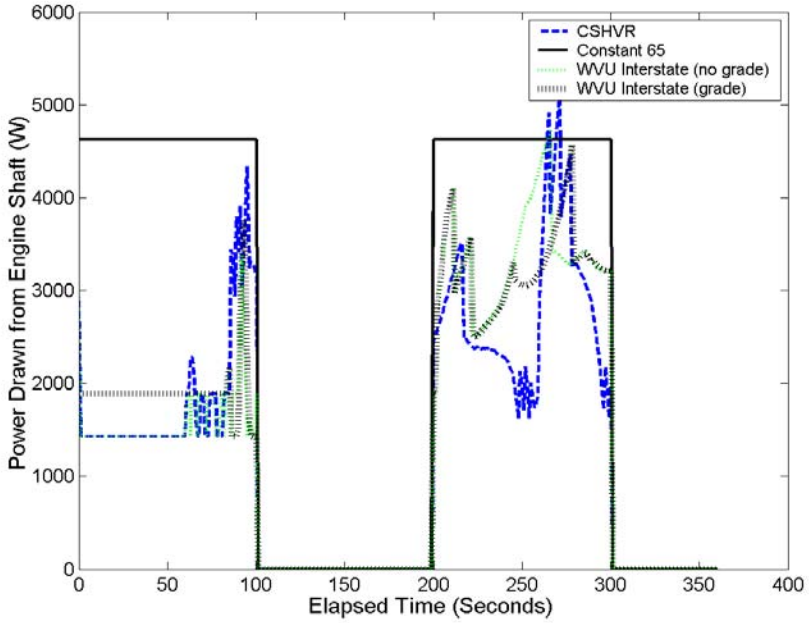

Figure 14 Air Conditioning Transient Load for First 360 sec of Drive Cycle

A final model example is now presented. Consider the 21st Century Truck tractor-trailer model with variable auxiliary loads over the CSHVR. Compare this run to a run with a constant mechanical load equal to the average of the variable load. The power consumed versus time is shown in Figure 15. The blue line corresponds to the auxiliary load of the speed-dependent load model. The black line is the constant auxiliary load model, which corresponds to the time average of the blue line.

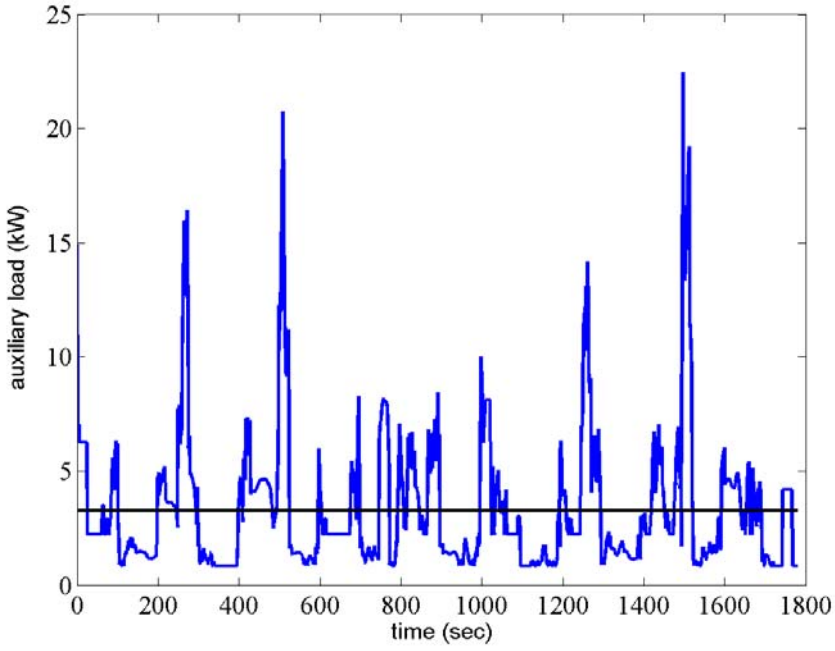

Figure 15 Variable Load vs. Constant Set at Average of Variable Load for Tractor-trailer Model over CSHVR

The average of the variable load in Figure 15 is 3.273 kW. This is the setting of the constant mechanical load. Figure 16 and Figure 17 give the miles per gallon and fuel use, respectively, over the CSHVR for the two models.

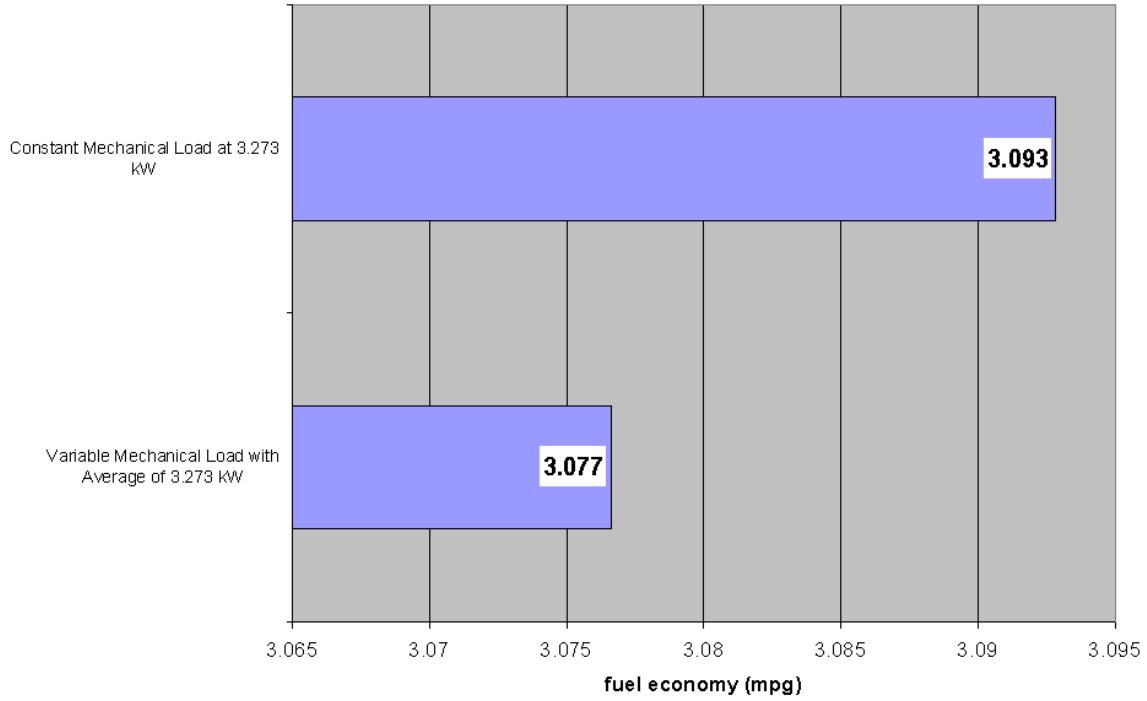

Figure 16 Miles Per Gallon over CSHVR for Constant vs. Variable Mechanical Load Model Run

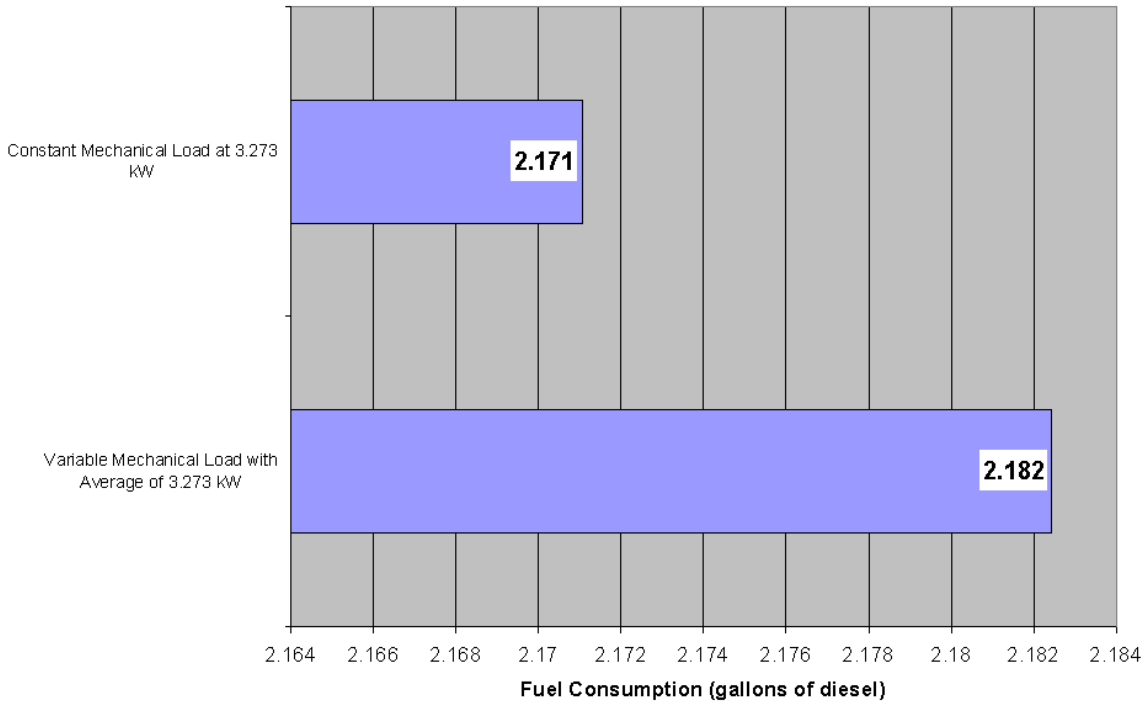

Figure 17 Gallons of Fuel Used over CSHVR for Constant vs. Variable Mechanical Load Model Run

There is a noticeable difference in fuel economy and fuel use between the two models. This difference can be partially explained by revisiting Figure 15. The standard deviation in the variable mechanical power signal is 2.861 kW. However, the minimum power point is only 0.856 standard deviations below the mean. In contrast, the maximum auxiliary load is more than 6.7 standard deviations above the mean.

This difference in standard deviations confirms what is shown in Figure 15: the variable mechanical load signal is not evenly distributed about the mean. Fuel use is accumulated over time (i.e., fuel rate multiplied by time spent at the fuel rate). The fuel economy of the variable mechanical load model is worse than that of the constant load model. Time spent high above the mean auxiliary load is shorter than time spent slightly below the mean. Evidently, time spent at high auxiliary load uses more fuel than can be offset by time at low auxiliary load.

3.1.2 Time-variable Electrical Loads

In addition to mechanical loads, ADVISOR can simulate electrical loads. On conventional vehicles, electrical loads are ultimately powered by an alternator, which is belt driven with the engine shaft. Thus, conventional electrical loads are ultimately mechanical loads. This connection is revisited as different alternator speed-load maps are applied.

Consider a truck with an average electrical load of 700 W (0.7 kW) and a peak load of 1000 W (1 kW) (SAE 2000). All other parameters are the same as the 21st Century Truck tractor-trailer model of Appendix A. For the baseline model, a constant mechanical load of 7.457 kW and constant electrical load of 700 W is used.

For the baseline run, the 700 W constant electrical load is applied through a constant 60% efficient alternator. Tabulated results for these conditions are given in Table 4 of Appendix A. The baseline loads in this example are smaller than in the previous example, which used 15 kW of mechanical loads.

To contrast with the aforementioned baseline model, a variable electrical load model is now presented. This model has a peak electrical load of 1 kW and average load of 0.7 kW. The profile consists of a 0.5 kW load for 60% of the time and a 1 kW load for 40% of the time. The tabulated results of this run are given in Appendix A, Table 5. The difference in fuel use over the drive cycle between the baseline and time-variant loads is shown in Figure 18.

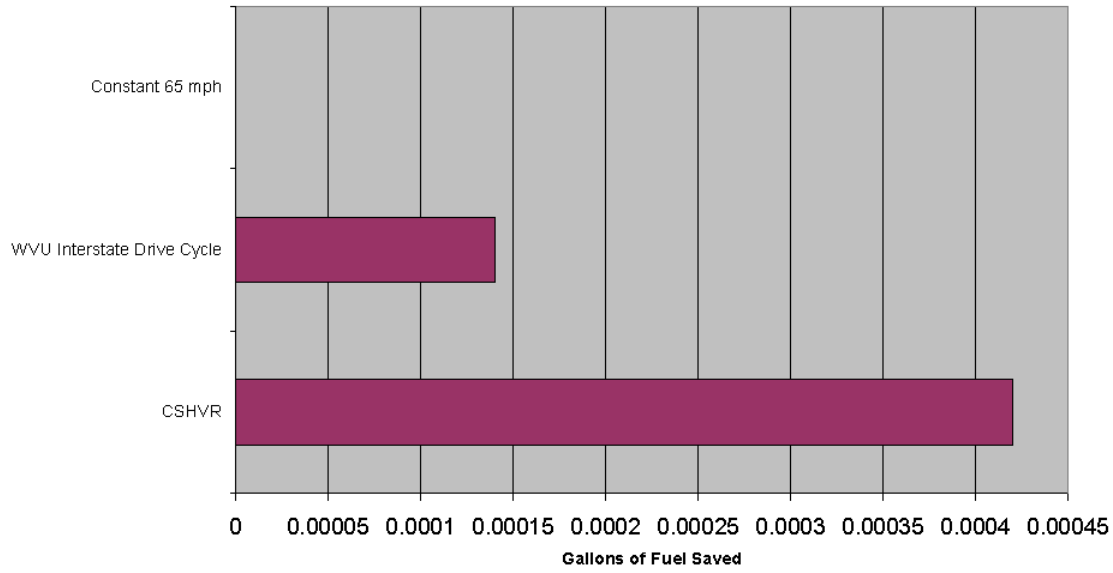

Figure 18 Difference in Predicted Fuel Use for Constant vs. Variable Electrical Loads

The difference in fuel economy between the models is minimal (Figure 18, Table 4 and Table 5 of Appendix A). This may result from the small magnitude of the electrical loads applied. In addition, the variable load signal may not be significantly different from the mean of that signal.

To explore differences in signal type, consider another variable electrical load profile. This profile runs with a 2-kW peak 35% of the time and no load 65% of the time. Thus, the average is still 0.7 kW. With this loading profile, a 3.0062-mpg fuel economy is achieved over the CSHVR. This is a difference in fuel economy of 0.005 gal over the CSHVR. Comparison to Figure 18 would suggest that this is significant. Thus, signal composition appears to be a factor in final fuel economy.

Another item that may affect the loading is alternator efficiency. In the baseline and variable electrical models, the alternator is assumed to be at a constant 60% efficiency. This is not realistic as alternator efficiency varies with load and engine speed. Recent data for a typical alternator are available (Schmidt *et al.* 2000). Results obtained by rerunning the models using a variable-efficiency generator appear in Table 6 of Appendix A. The effect that alternator efficiency has on power use can be seen by comparing Figure 19 with Figure 20. Even with a more realistic alternator model, differences between a cyclic load and the average of that load are small (Table 6, Appendix A).

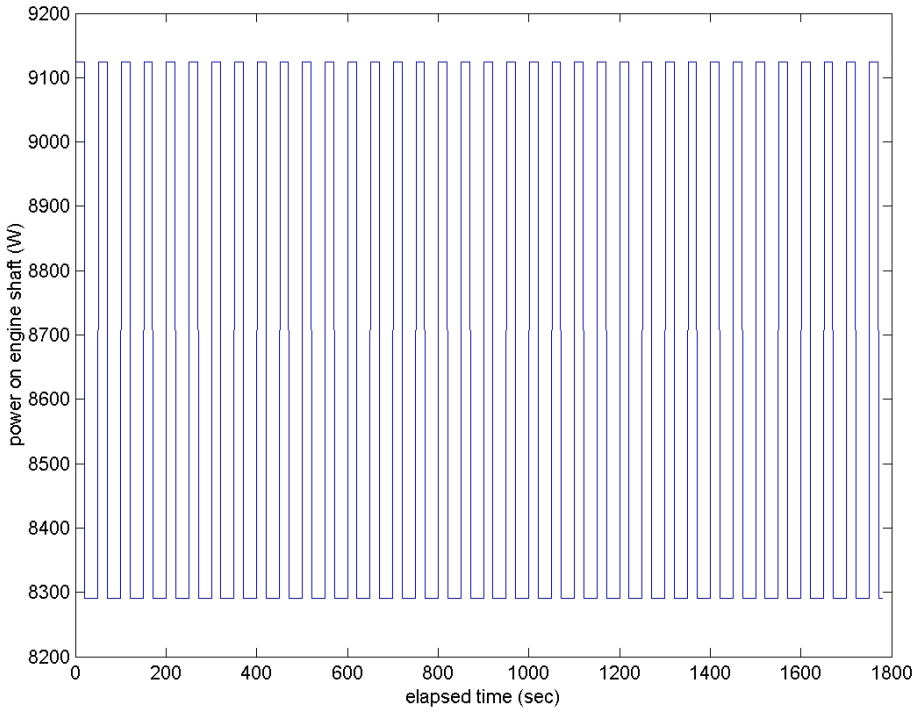

Figure 19 Auxiliary Load on Engine vs. Time with a Constant 60% Efficient Alternator

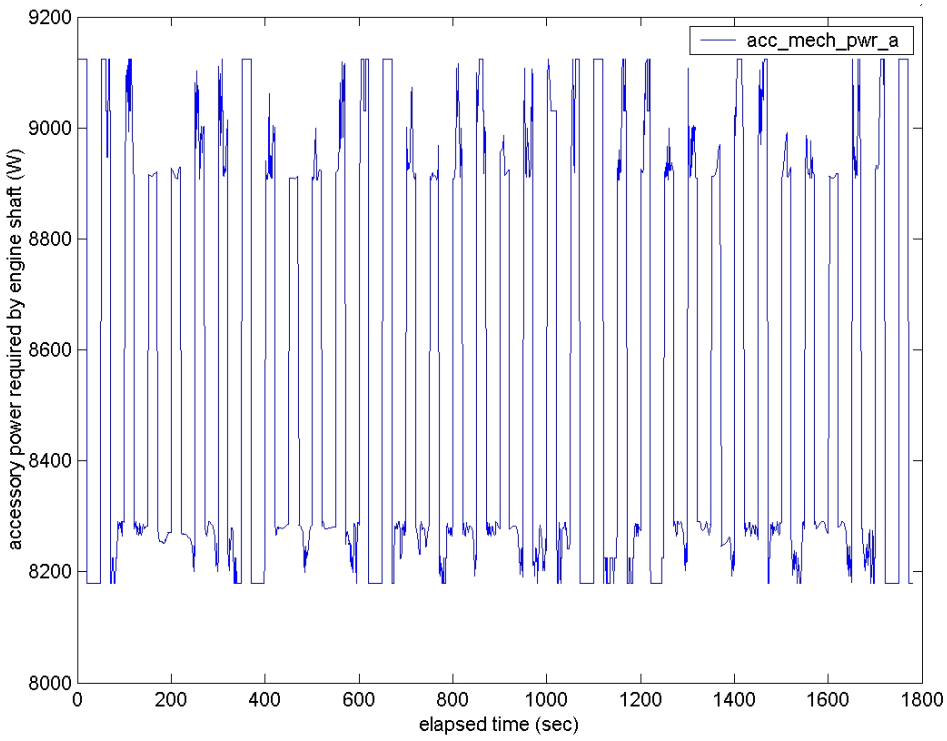

Figure 20 Auxiliary Load on Engine vs. Time with a Variable-efficiency Alternator

There are several reasons for the fuel differences between time-variable electrical load and constant load models. First, the modeling example places a 0.7 kW average load on a

332 kW truck engine. So much fuel is used to move the 80,000-lb vehicle that the fuel used for electrical accessories is difficult to detect.

Second, there is the difference between speed-dependent mechanical loading and constant loading at the average power (see end of section 4.1.1). For mechanical loading, there was an unbalance around the mean (i.e., a handful of points were far above the mean for a brief amount of time). Most operating points were below the mean for most of the time. In contrast, the electrical load profiles used here (Figure 19 and Figure 20) are very evenly distributed about their mean power values.

Third, speed-dependent mechanical loads reach a different cycle average per drive cycle for the same device loading profile. In contrast, the electrical load models are mostly decoupled from the drive cycle. Exceptions include electrical loads tied directly to the driving profile (e.g., brake lights).

3.2 Saber Co-simulation of Electrical Loads

Saber is a simulation package offered by Synopsys (formerly Avant!). It can be used to evaluate circuit, module, and electrical component designs and electrical systems on a detailed level. Co-simulation of ADVISOR with Saber is an ongoing project with Delphi Automotive Systems (MacBain and Conover 2000, MacBain and Conover 2001, MacBain and Conover 2001a, MacBain *et al.* 2001, ADVISOR 2002, Johnson *et al.* 2001).

To demonstrate the capabilities of Saber, a Saber co-simulation with ADVISOR was conducted. The model results are discussed here and tabulated in Table 7, Appendix A. The basic vehicle platform used is the 21st Century Truck tractor-trailer model mentioned in section 4.1.2 and Appendix A.

Saber co-simulation works by passing state information back and forth between Saber and ADVISOR (MATLAB/Simulink) at specified time steps. The Saber model consists of the entire electrical system including the alternator. The default alternator is a constant 60% efficiency unit. Figure 21 is a schematic of the electrical system modeled by Saber.

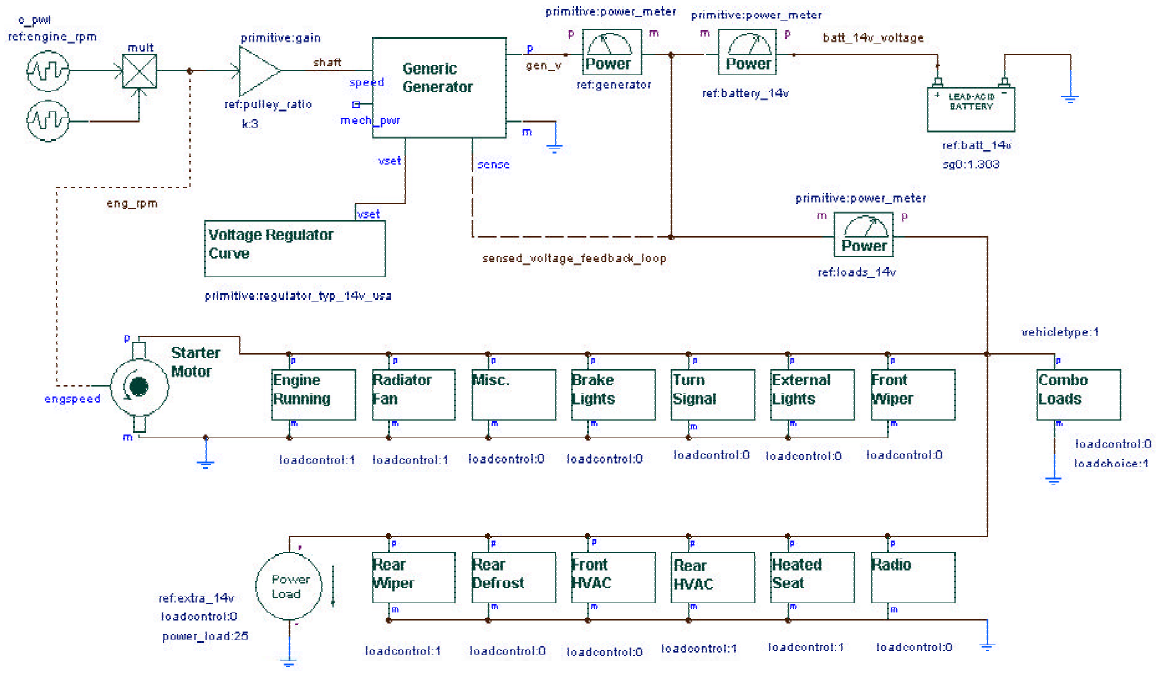

Figure 21 Saber Schematic of Conventional Vehicle 14-V Electrical System (Saber-ADVISOR Co-simulation)

Because of the time required to run a Saber co-simulation, only one run over the CSHVR is presented. Predicted fuel economy from ADVISOR time-variable electrical loading, constant electrical loading, and Saber co-simulation are presented in Figure 22. Only the CSHVR cycle results are given.

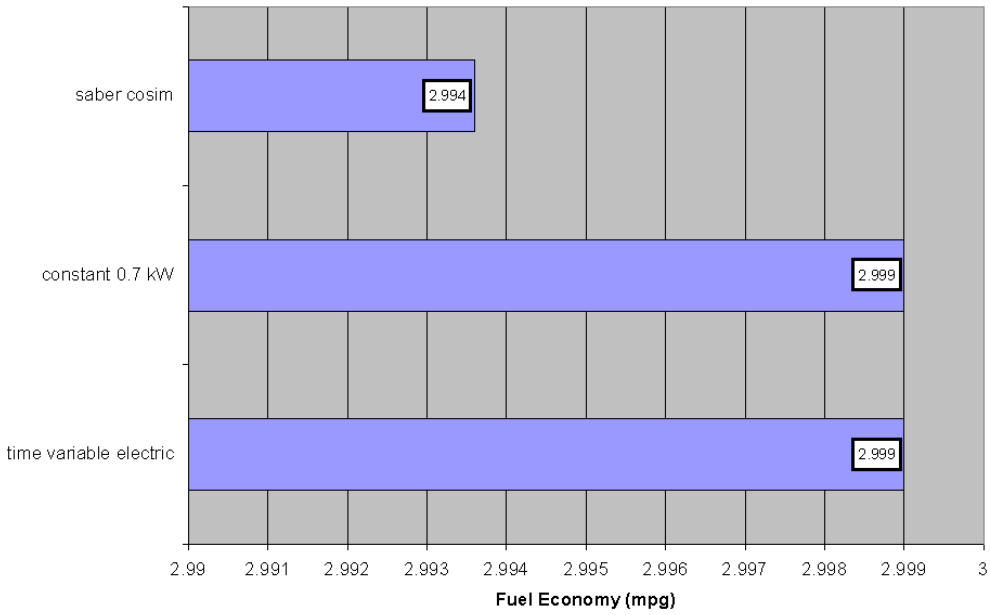

Figure 22 Predicted Fuel Economy Using Three Different Auxiliary Load Models over CSHVR Drive Cycle

The three models predict similar fuel economies. However, the Saber model predicts a slightly lower fuel economy than the other two models. This may be due to the Saber battery model.

Saber adds additional information on the electrical system to what is normally available through ADVISOR. This includes time-histories for the starting-lighting-ignition battery state-of-charge (SOC) and electrical bus voltage and power. Battery SOC and current versus time for the Saber co-simulation run are shown in Figure 23 and Figure 24.

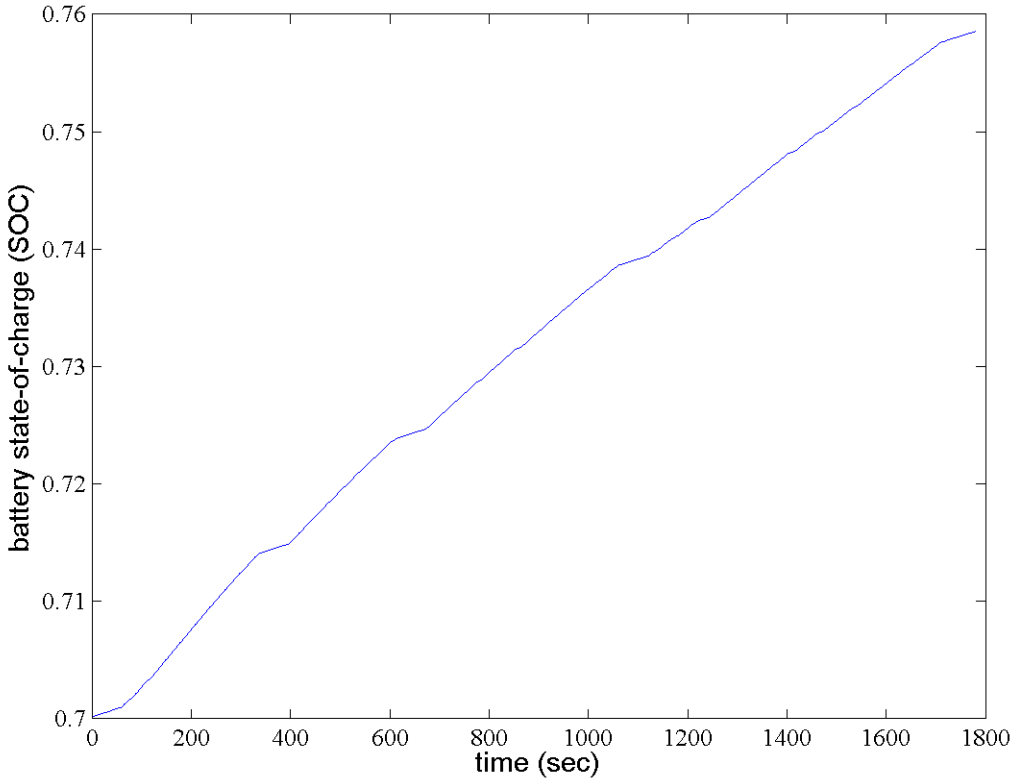

Figure 23 Starting-lighting-ignition Battery SOC History during CSHVR

During this run, the battery SOC increases over the cycle. This increase in SOC places a small extra burden on the engine. This may explain why the Saber co-simulation's predicted fuel economy is lower than the ADVISOR electrical load models. Figure 24 shows another Saber-specific variable—electrical current over the 14-V power bus versus time.

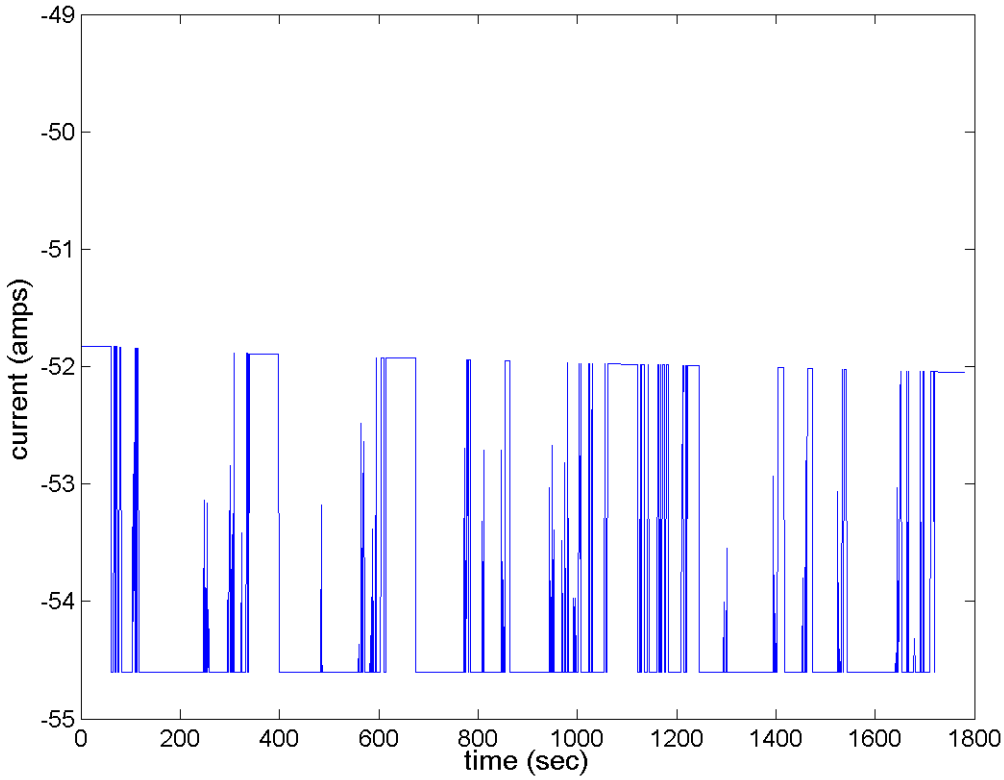

Figure 24 Current History of Power Bus over CSHVR

Currently, Saber models for conventional single-voltage and duel-voltage systems exist. NREL is currently working with Delphi on Saber models for series and parallel drive trains. These models will simulate all electronic components within Saber (e.g., motor, generator, and energy storage).

3.3 SINDA/FLUINT Co-simulation

SINDA/FLUINT is a software code used to analyze thermal-fluid systems. SINDA/FLUINT has been used previously at NREL to model automotive A/C systems (Hendricks 2001a, Hendricks 2001b, Cullimore and Hendricks 2001). SINDA/FLUINT A/C models have been used in conjunction with ADVISOR to predict fuel economy impact and to perform system optimizations.

SINDA/FLUINT co-simulation is similar to Saber co-simulation. SINDA/FLUINT and ADVISOR (MATLAB/Simulink) pass information back and forth at designated time intervals. During a simulation, ADVISOR runs for one time step, then SINDA/FLUINT, then ADVISOR, and so on. Critical parameters are exchanged between ADVISOR and SINDA/FLUINT at each time step. These parameters include co-simulation control parameters, A/C system operation parameters, and model outputs and results.

In this section, an A/C system for an International truck is presented. The SINDA/FLUINT graphical interface depicting the A/C loop is shown in Figure 25. This

particular SINDA/FLUINT A/C model is a stand-alone model. It can be simulated over the SC03 vehicle drive cycle (Figure 26) or any other drive cycle of interest.

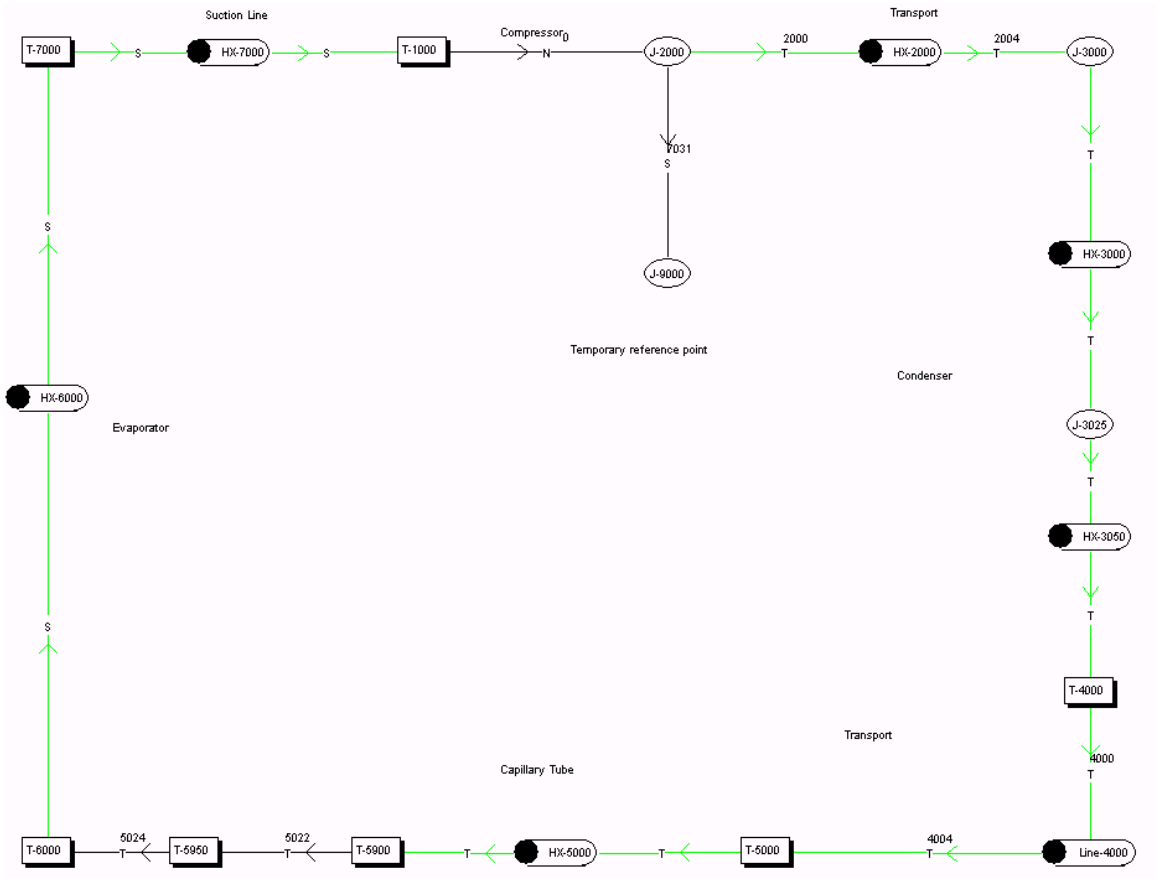

Figure 25 SINDA/FLUINT Transient A/C Loop for Class 6 Truck Cabin

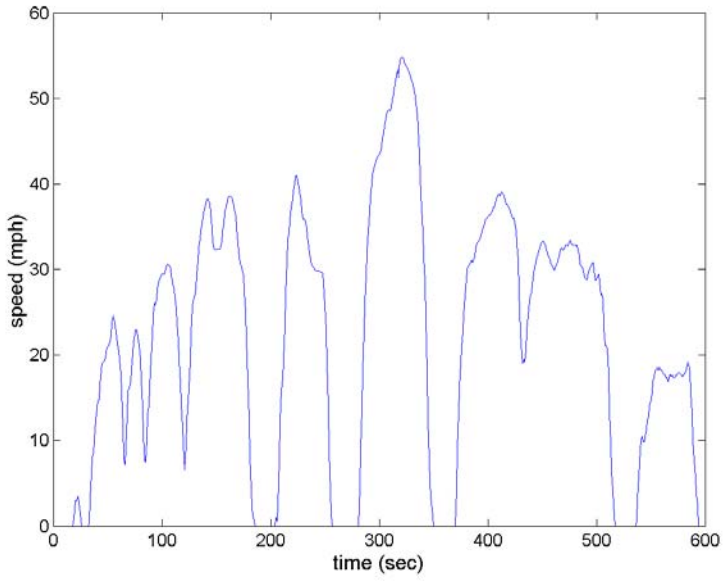

Figure 26 The SC03 Drive Cycle

The SINDA/FLUINT model contains an important sub-model representing and simulating the vehicle cabin thermal environment. The cabin sub-model allows one to simulate and monitor cabin conditions during the A/C system's transient operation.

In running the SINDA/FLUINT transient A/C model over the SC03 drive cycle, a wealth of thermodynamic properties is available. Figure 27 depicts the cooling of a cabin during the SC03. The cabin is under extreme conditions of high ambient temperature and high solar loading. However, the A/C system is able to cool the cabin quickly to approximately 75^{o}F.

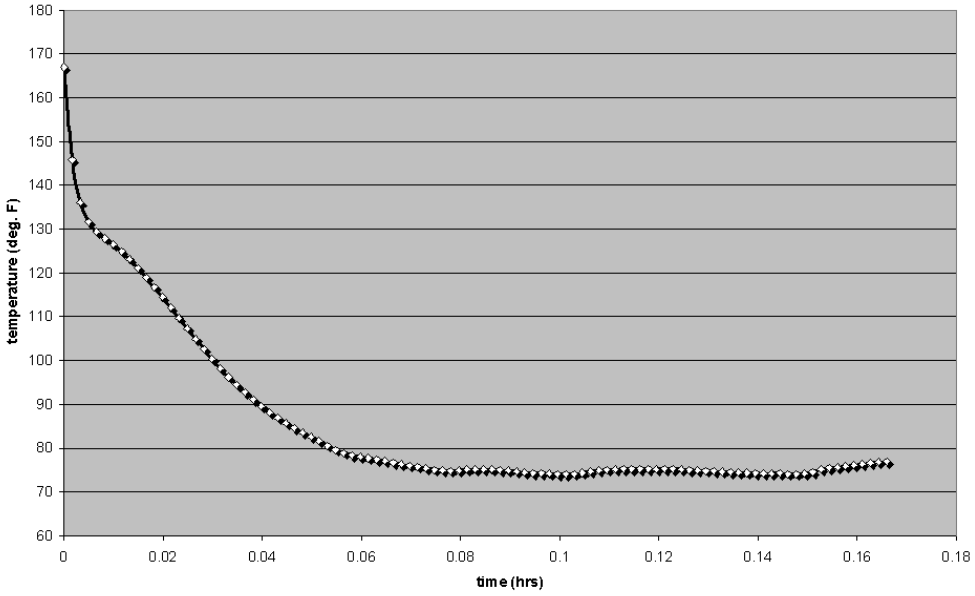

Figure 27 Predicted Cabin Temperature vs. Time over the SC03 Drive Cycle

The air temperatures into and out of the A/C evaporator over the SC03 cycle are shown in Figure 28. The slight increase in temperature at the outlet of the evaporator is due to moisture removal.

The power required by the A/C air compressor over the cycle is shown in Figure 29. The air compressor responds to the transient SC03 drive cycle because the compressor is belt driven off the engine. The approximation of compressor shaft speed used in the SINDA/FLUINT stand-alone model is very basic. The ADVISOR-SINDA/FLUINT co-simulation is more realistic because it uses a more detailed drive train model.

Figure 30 through Figure 37 show the thermodynamic state of the A/C model versus time. In Figure 37, the location of phase change in the condenser (two-phase flow) can be estimated.

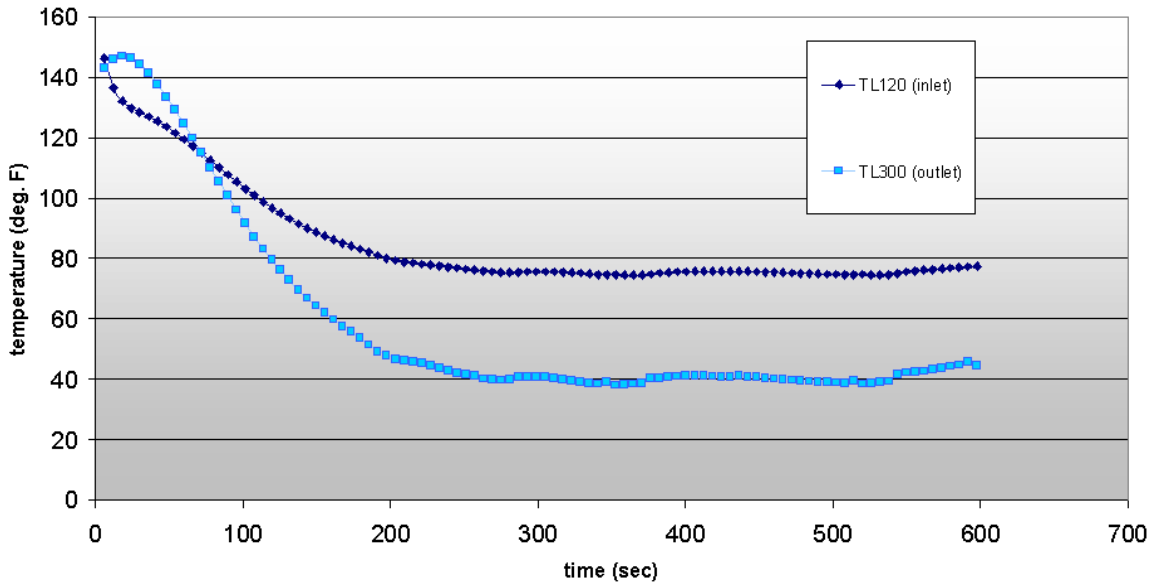

Figure 28 Predicted Air Temperatures into and out of the Evaporator over the SC03 Drive Cycle

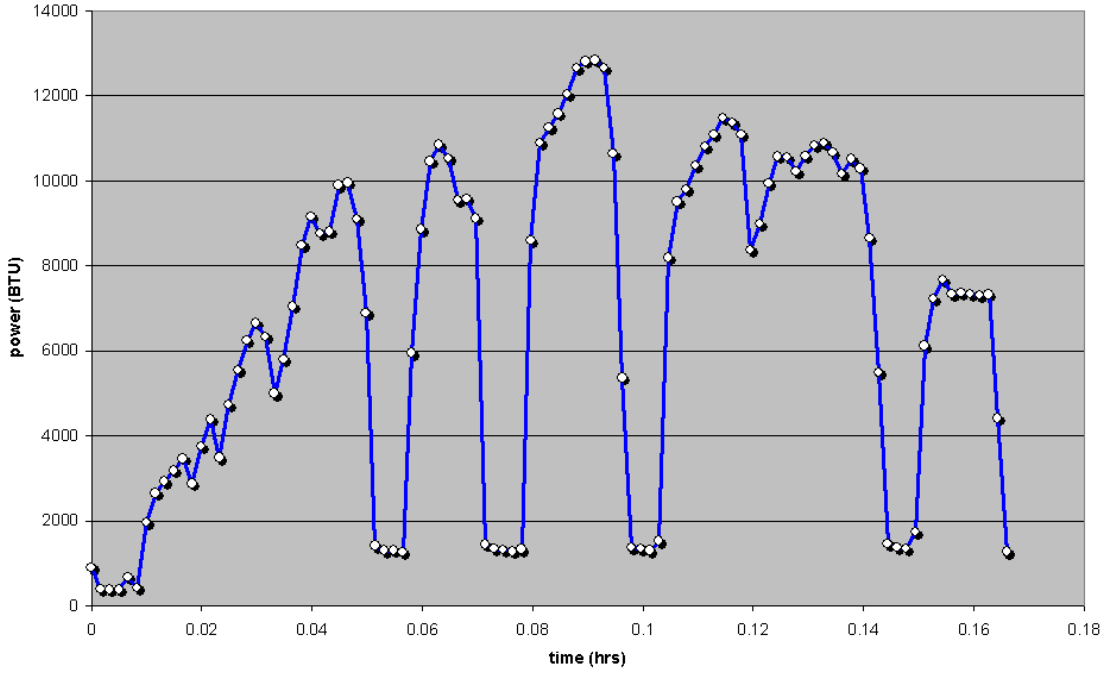

Figure 29 A/C Compressor Power over the SC03 Drive Cycle

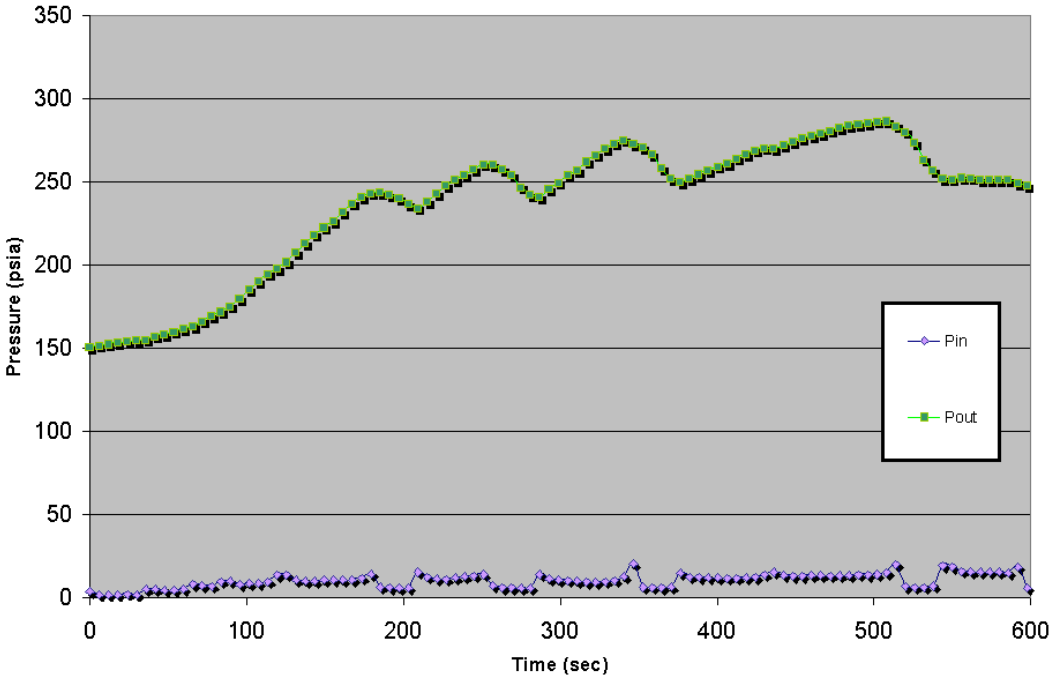

Figure 30 Predicted High and Low Pressures along the A/C Loop vs. Time over the SC03 Drive Cycle

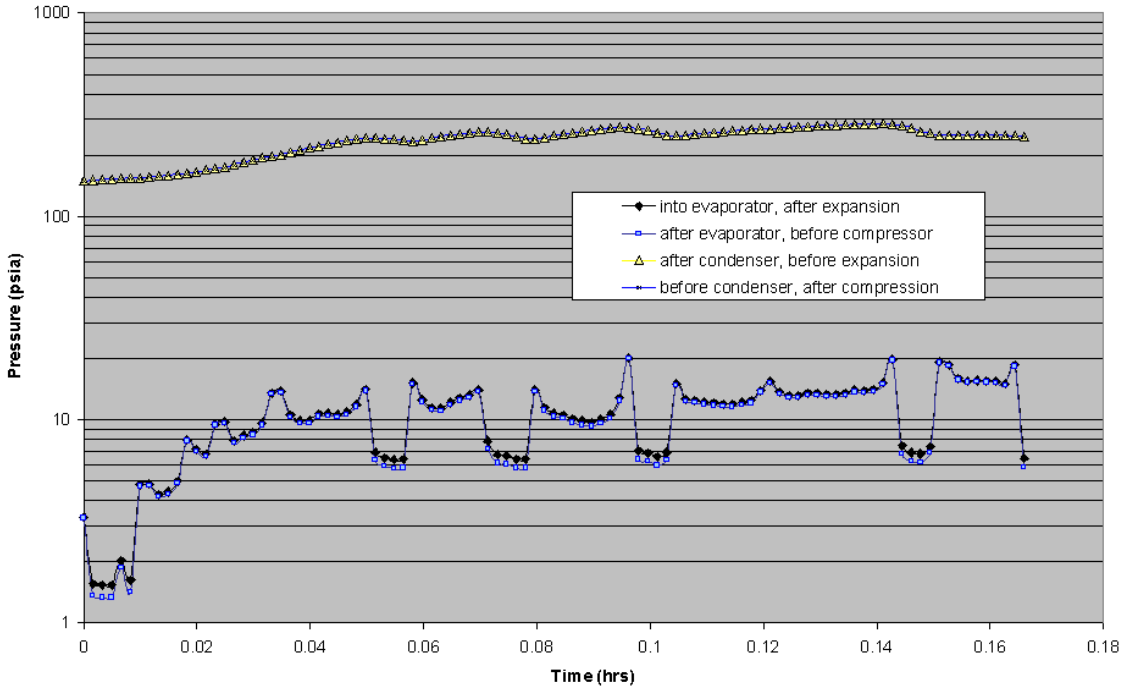

Figure 31 A/C Loop Pressures on a Semi-log Scale vs. Time over SC03 Drive Cycle

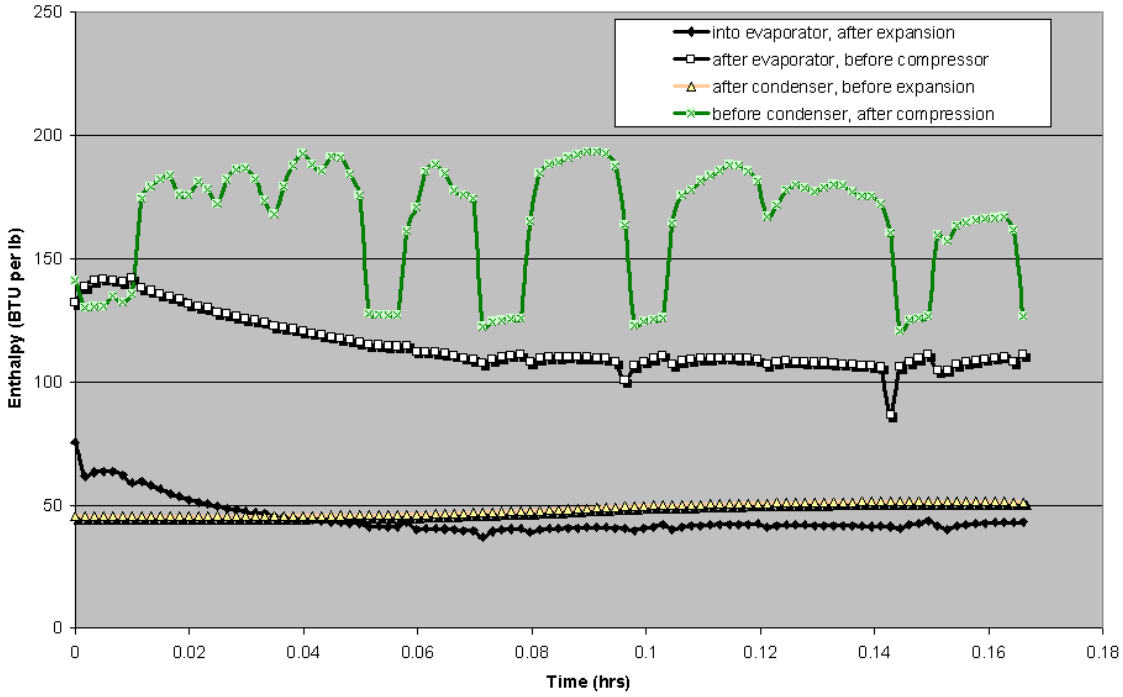

Figure 32 Enthalpy at Various Points around the A/C Loop vs. Time

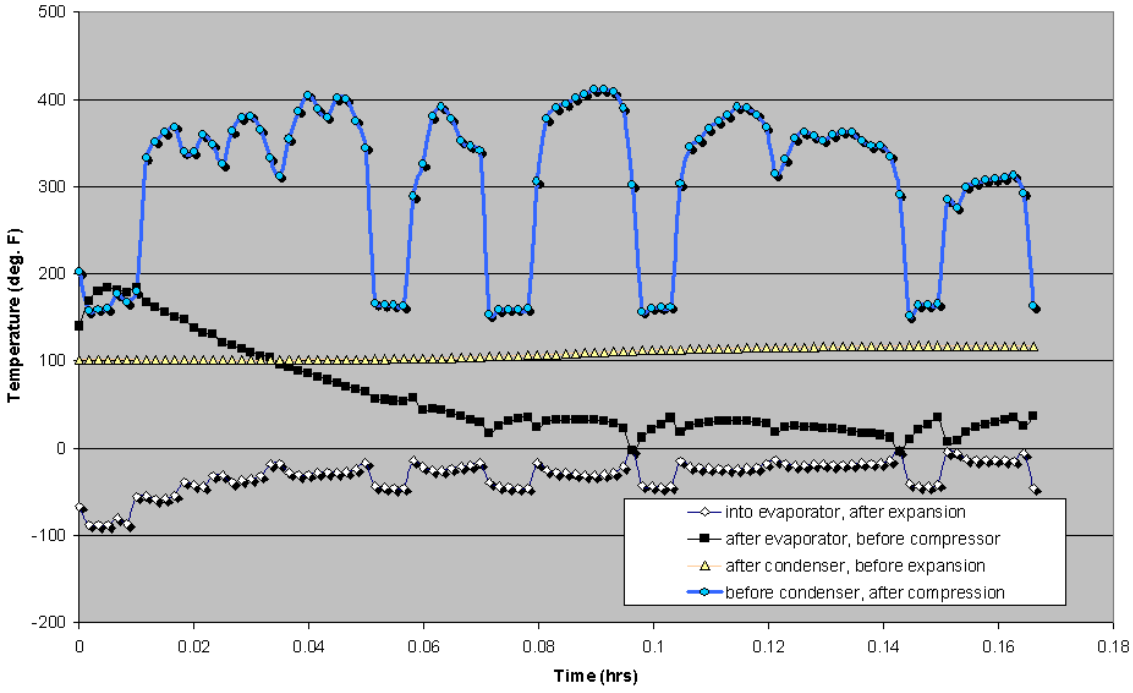

Figure 33 Temperatures at Various Points around the A/C Loop vs. Time

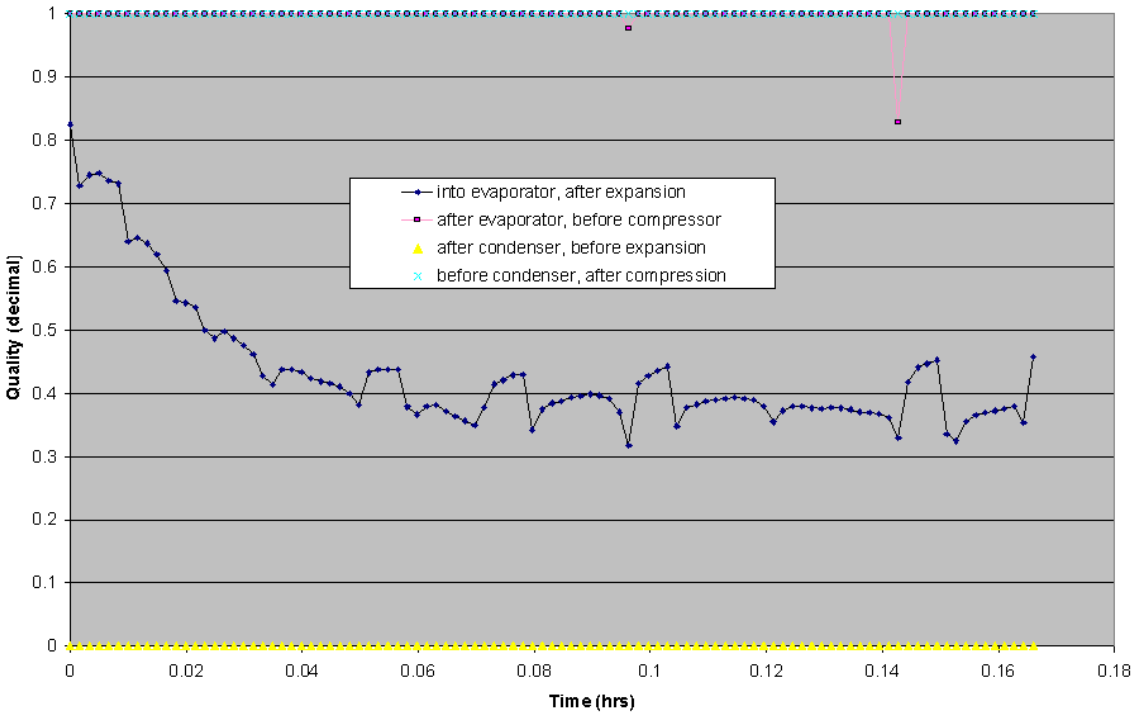

Figure 34 Quality at Various Points around the A/C Loop vs. Time

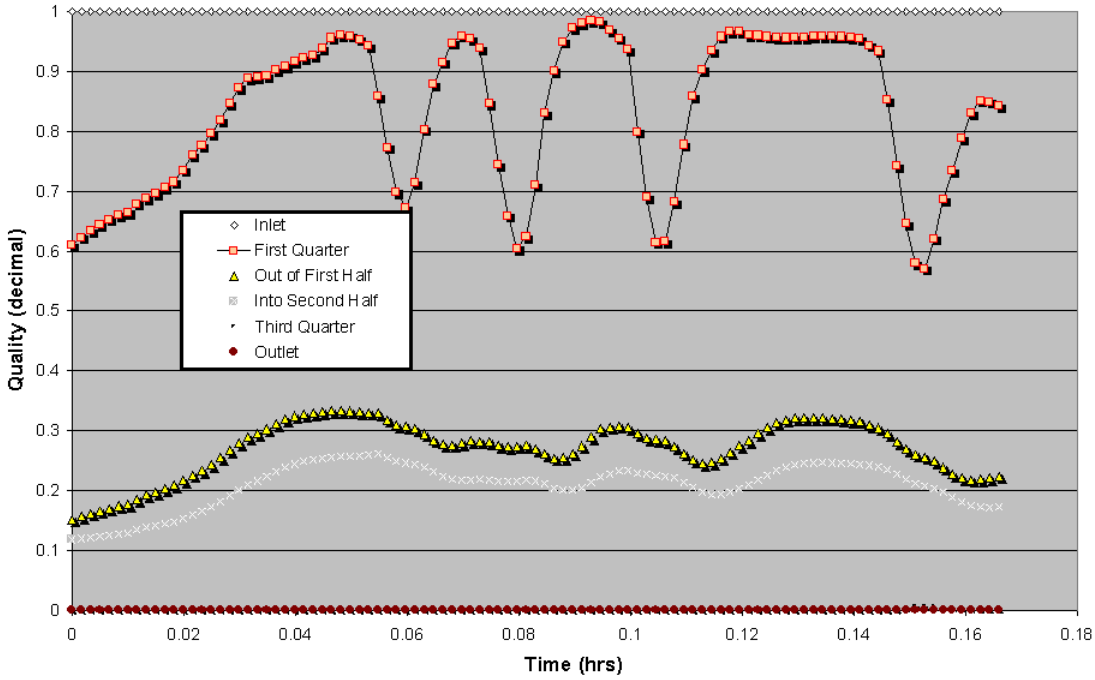

Figure 35 Quality at Various Points through the Condenser vs. Time

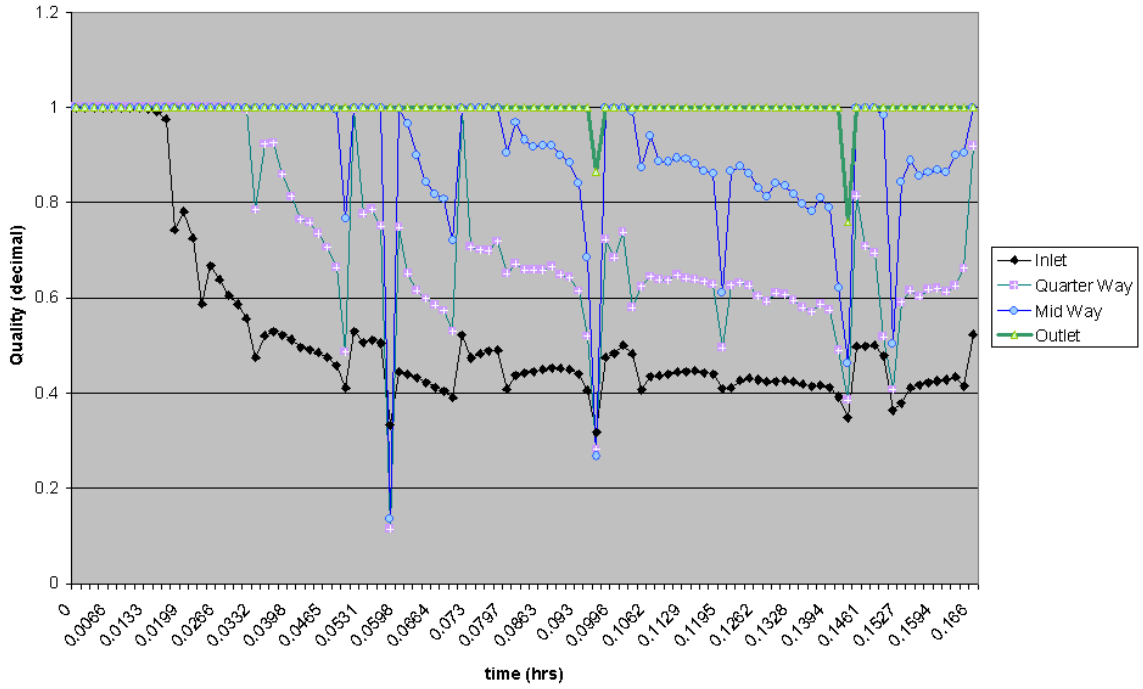

Figure 36 Quality at Various Points through the Evaporator vs. Time

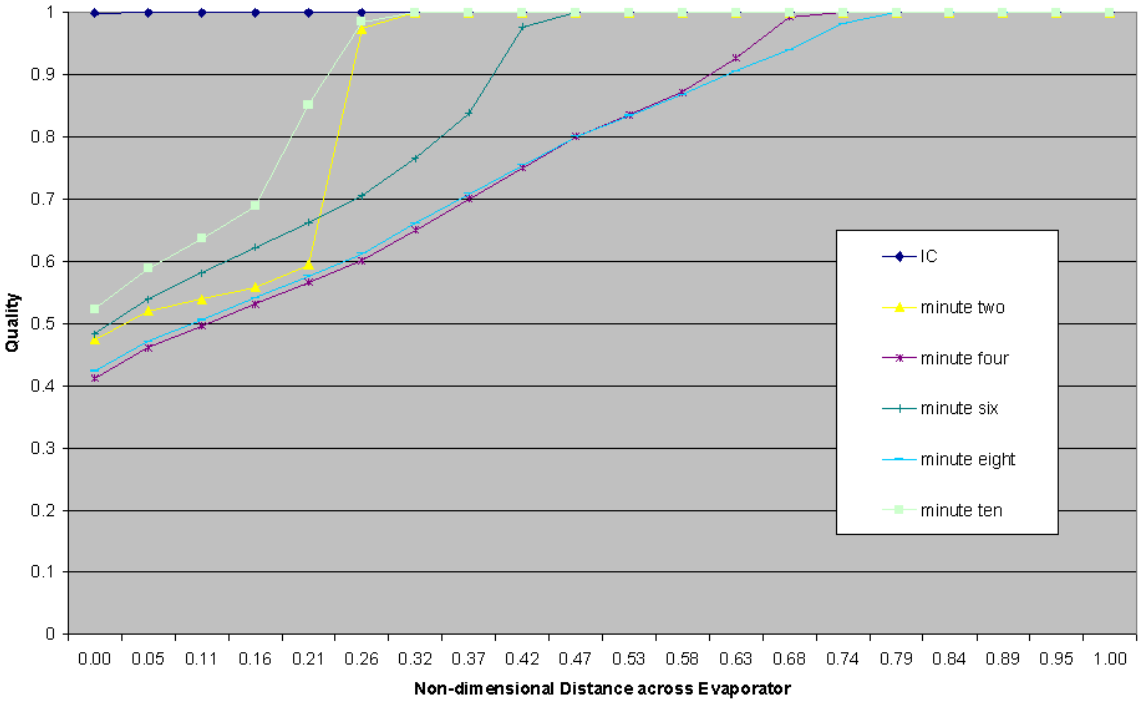

Figure 37 Quality by Length through the Evaporator at Various Times along the SC03 Drive Cycle

Figure 38 depicts the operation points of the A/C model on an enthalpy versus semi-log pressure chart. The vapor dome for R134a is given for reference.

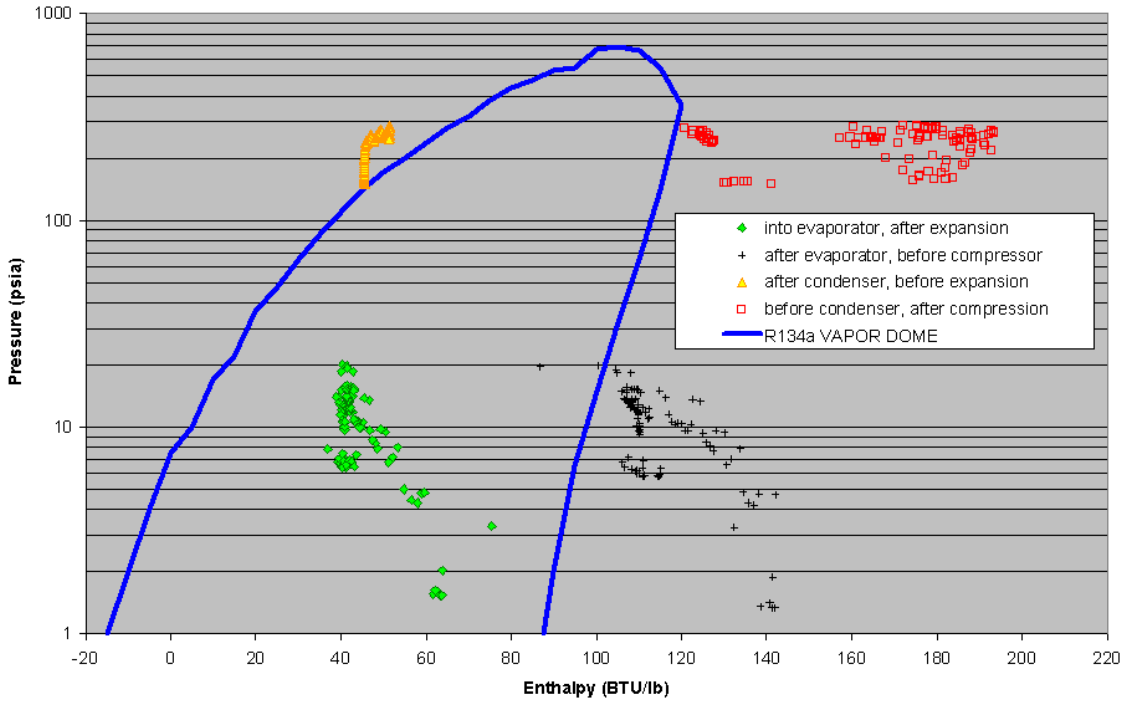

Figure 38 Pressure-enthalpy Diagram Depicting the Regions of Operation of Four Points in the A/C System Superimposed over the R-134a Vapor Dome

Note that the thermodynamic operational points in Figure 38 are not constant with time. The conventional automotive vapor compression cycle nominally runs as a dynamic system. Compressor speed, air flows, ambient air temperature, and cabin conditions are constantly changing. Therefore, system P-h points are dynamic as system external inputs and conditions change. Design and analysis assuming constant conditions is therefore both inaccurate and inappropriate.

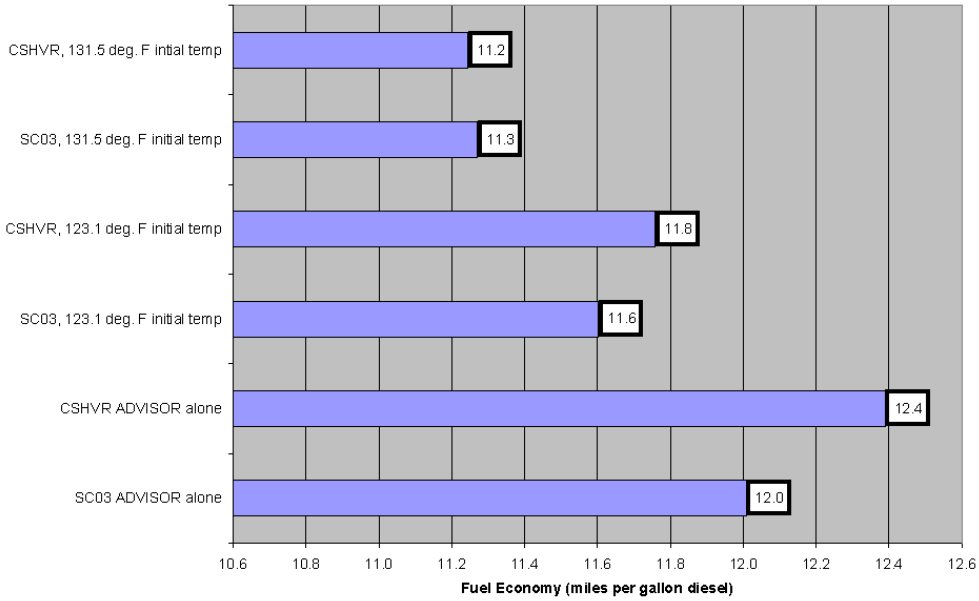

Figure 39 Fuel Economy Predicted by ADVISOR-SINDA/FLUINT Co-simulations with Designated Starting Conditions

To tie A/C performance back to vehicle fuel economy, a co-simulation with ADVISOR can be performed. A quick study was performed with two drive cycles—CSHVR (Figure 1) and SC03 (Figure 26)—for A/C on a truck. Two initial cabin temperatures were examined: 131.5°F and 123.1°F. The fuel economies predicted for the baseline ADVISOR-only vehicles and ADVISOR-SINDA/FLUINT A/C vehicles are shown in Figure 39. The A/C system is held constant throughout the study. Only the initial cabin temperature and subsequent drive cycle are varied. Cabin cooling profiles are shown in Figure 40.

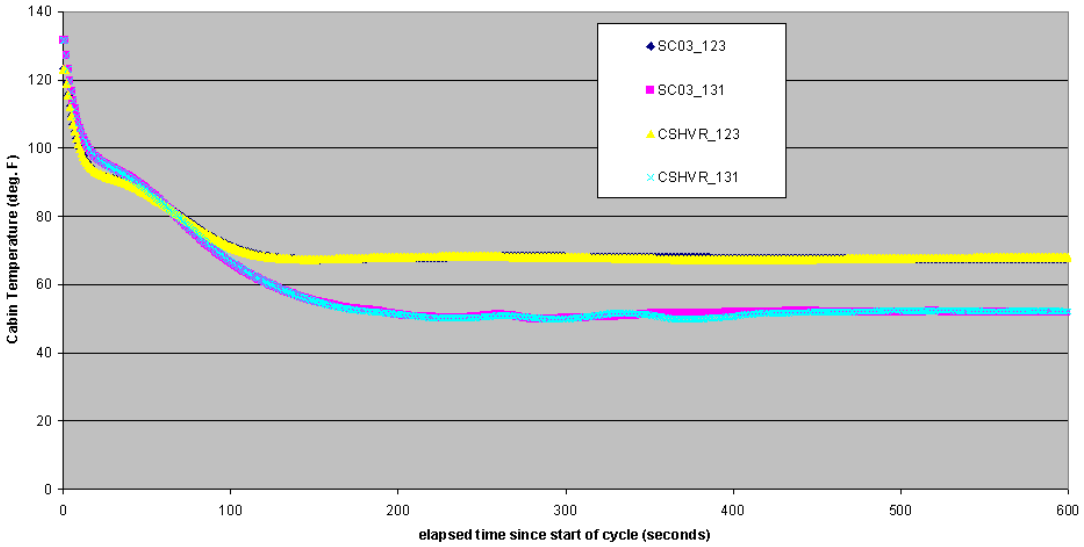

Figure 40 Cabin Temperature vs. Time for the ADVISOR-SINDA/FLUINT Co-simulation with Two Starting Temperatures (123 F and 131 F) and Two Drive Cycles (CSHVR and SC03)

3.4 Thermoelectric Models

Thermoelectric materials convert thermal energy into electricity. The performance of thermoelectric materials is measured in terms of a "dimensionless figure of merit" written as "ZT." The figure of merit is expressed in Equation 1 (NASA 2001, Yao *et al.* 2001).

Equation 1 Figure of Merit

$$ZT = \frac{S^2 T}{\rho \lambda}$$

In Equation 1, ρ is electrical resistivity, T is absolute temperature, S is the Seebeck coefficient, and λ is thermal conductivity.

By coupling a thermoelectric device with a vehicle's exhaust stream, some waste energy can be recovered as electricity. A simple thermoelectric device is shown in Figure 41. A more advanced device using several different materials on the *p* and *n* legs is shown in Figure 42.

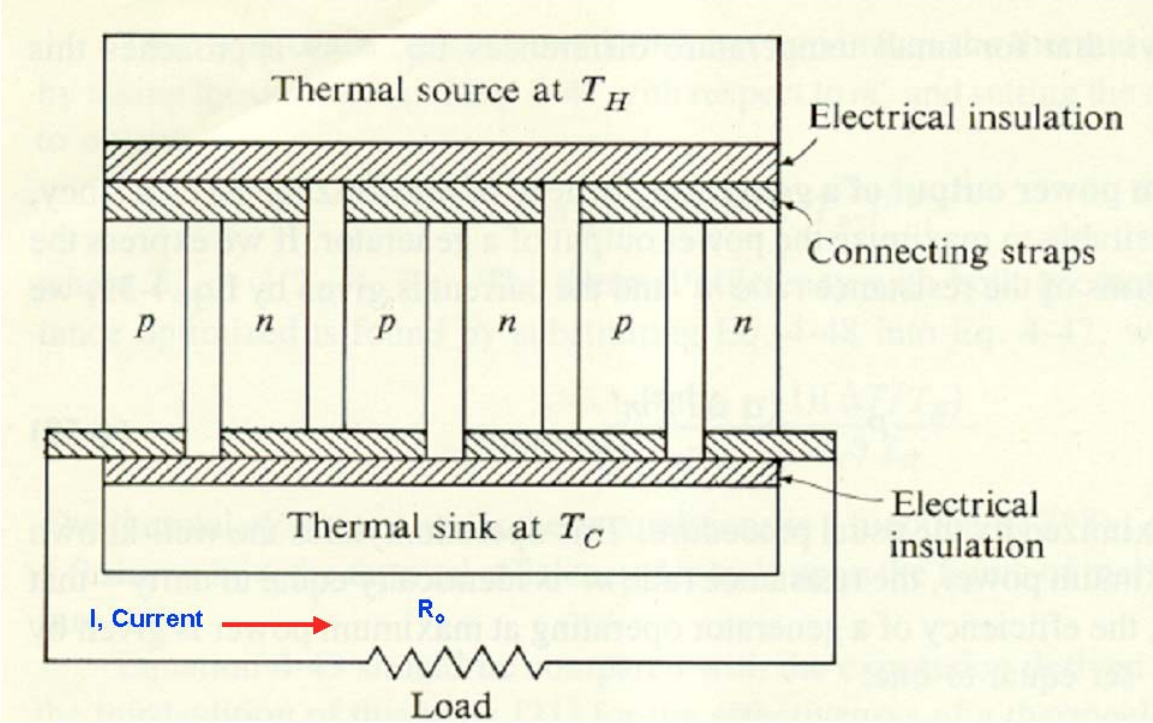

Figure 41 Thermoelectric Element

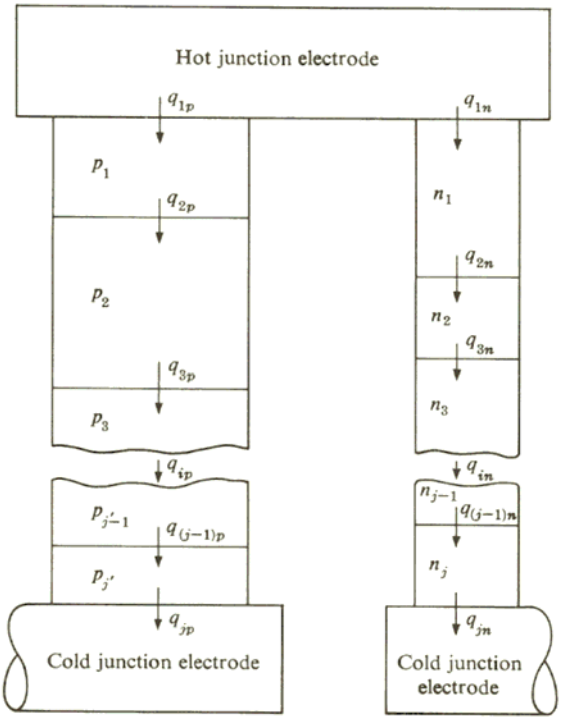

Figure 42 Thermoelectric Device with Multi-material Legs

Thermoelectric material characteristics are key inputs for NREL's thermoelectric models. These data show how ZT changes with temperature for various *n*-type (electron-donor) and *p*-type (electron-acceptor) thermoelectric materials. Examples of ZT versus temperature characteristics for various *n*- and *p*-type materials are shown in Figure 43 and Figure 44.

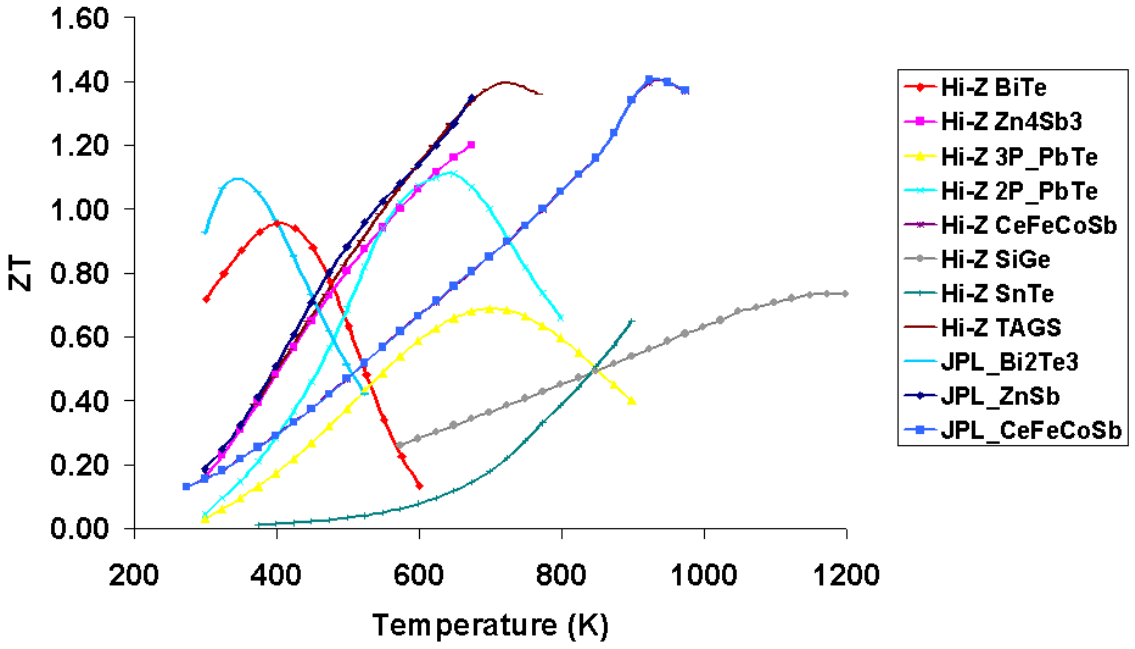

Figure 43 *p*-type Material ZT vs. Temperature Characteristics

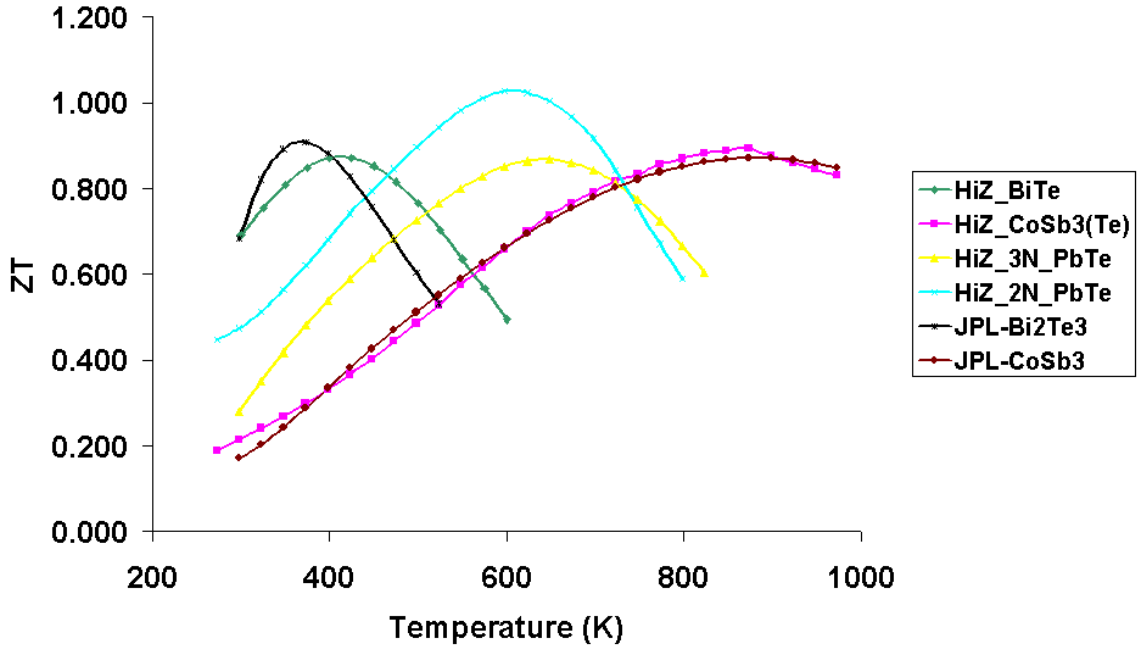

Figure 44 *n*-type Material ZT vs. Temperature Characteristics

NREL's thermoelectric models use the effectiveness-NTU method to model exhaust flow heat exchange (Incropera and DeWitt 1990). This results in a series of non-linear equations in temperature, which are solved numerically via a Newton-Raphson method for a range of hot-side/cold-side temperatures.

Realistic values for engine thermal states are required to generate useful thermoelectric model results. One source of information is a 10-L turbo-compressor–equipped compression-ignition (CI) engine model from WAVE (see section 3.6). Information from engine manufacturers is also useful.

With the 10-L CI engine model from WAVE, exhaust stream mass-flow rates and temperatures were predicted for a 65-mph highway cruising condition. The resulting maximum power and cold-side mass flow rate requirements were predicted with the thermoelectric model. These results are shown in Figure 45 and Figure 46.

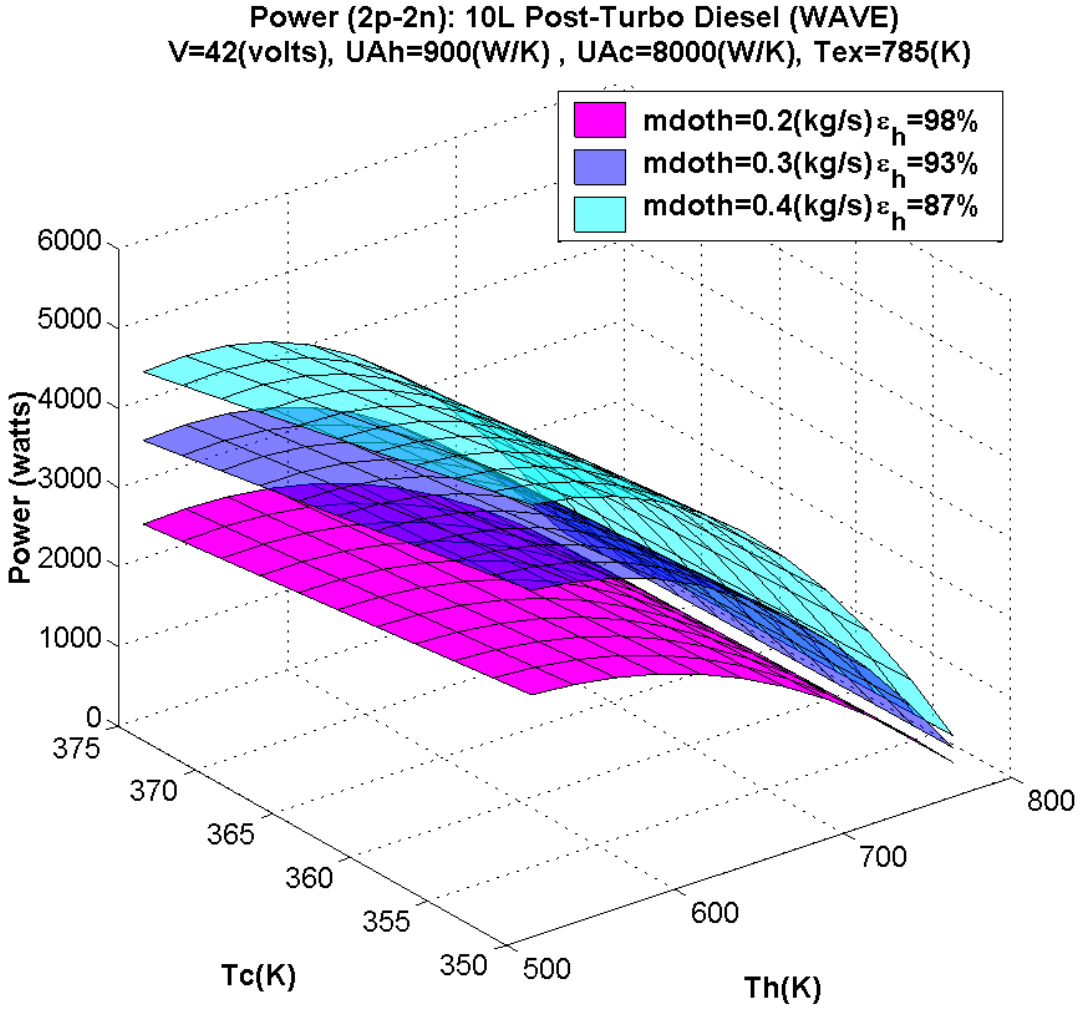

Figure 45 Predicted Electrical Power Available from Skutterudite-Bi_2Te_3 and $CoSb_3$-Bi_2Te_3 (NASA-Jet Propulsion Laboratory, Pasadena, CA) Thermoelectric Material Operating at the Given Hot- and Cold-side Temperatures and Exhaust Mass Flow Rates

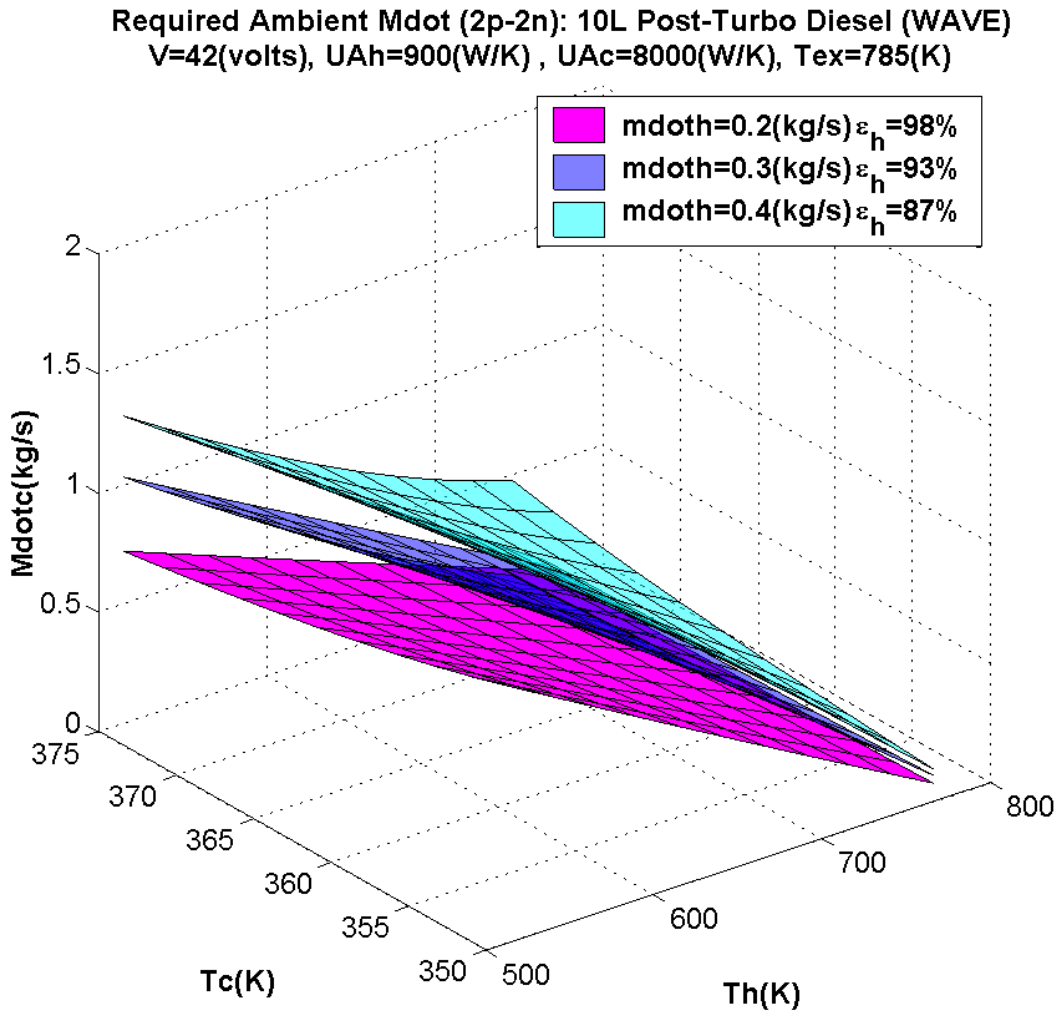

Figure 46 Required Cold-side Mass Flow Rates from Skutterudite-Bi_2Te_3 and $CoSb_3$-Bi_2Te_3 (NASA-Jet Propulsion Laboratory, Pasadena, CA) Thermoelectric Material Operating at Peak Power at the Given Hot- and Cold-side Temperatures and Exhaust Mass Flow Rates

Using the thermoelectric model, several "what-if" analyses can be performed for different materials and material combinations. For the 10-L CI engine above, a better solution is available using different materials. This new thermoelectric system requires 28% lower cold-side mass flow for essentially the same power. Results from this thermoelectric analysis are shown in Figure 47 and Figure 48.

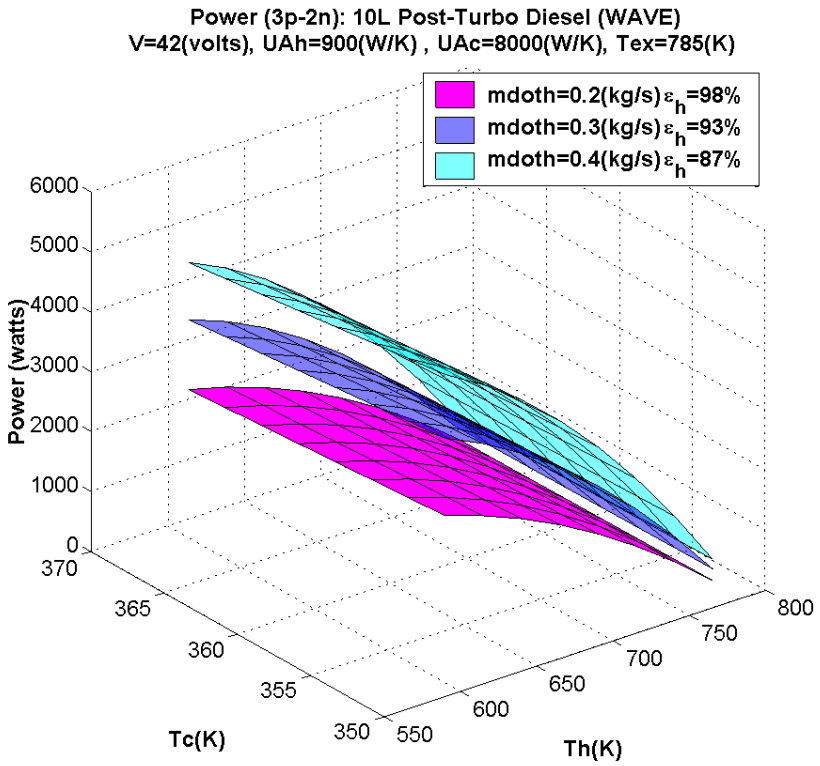

Figure 47 Predicted Electrical Power Available from a Skutterudite-Zn_4Sb_3-Bi_2Te_3 and $CoSb_3$-Bi_2Te_3 Thermoelectric Material Operating at the Given Hot- and Cold-side Temperatures and Exhaust Mass Flow Rates

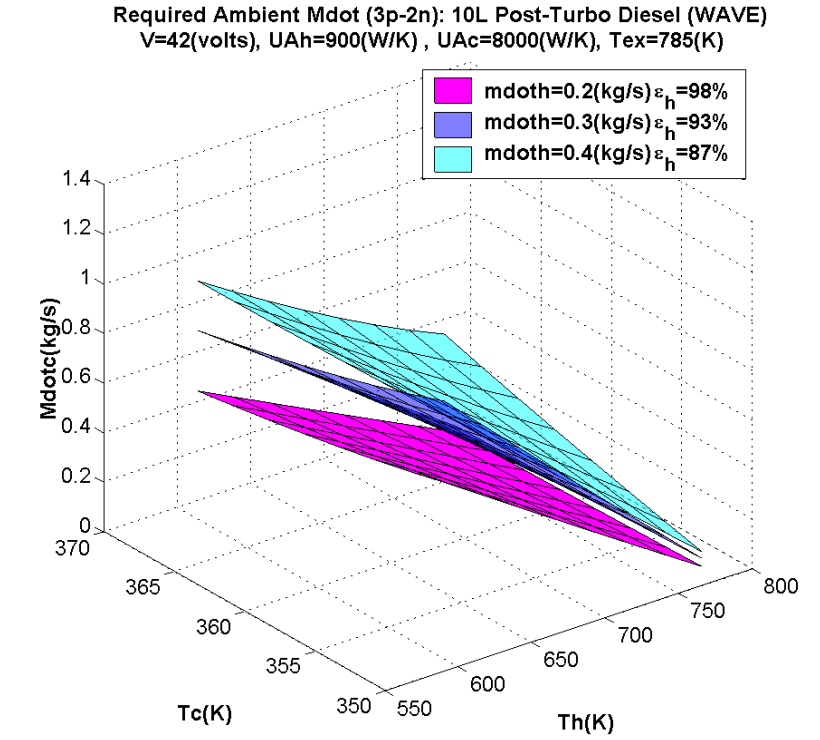

Figure 48 Required Cold-side Mass Flow Rates from a Skutterudite-Zn_4Sb_3-Bi_2Te_3 and $CoSb_3$-Bi_2Te_3 Thermoelectric Material Operating at Peak Power at the Given Hot- and Cold-side Temperatures and Exhaust Mass Flow Rates

Figure 49 is another interesting plot that can be generated from the thermoelectric model. The peak power output does not occur at the maximum efficiency of 9%–10%. Instead, efficiency at maximum power output is 4%–6%.

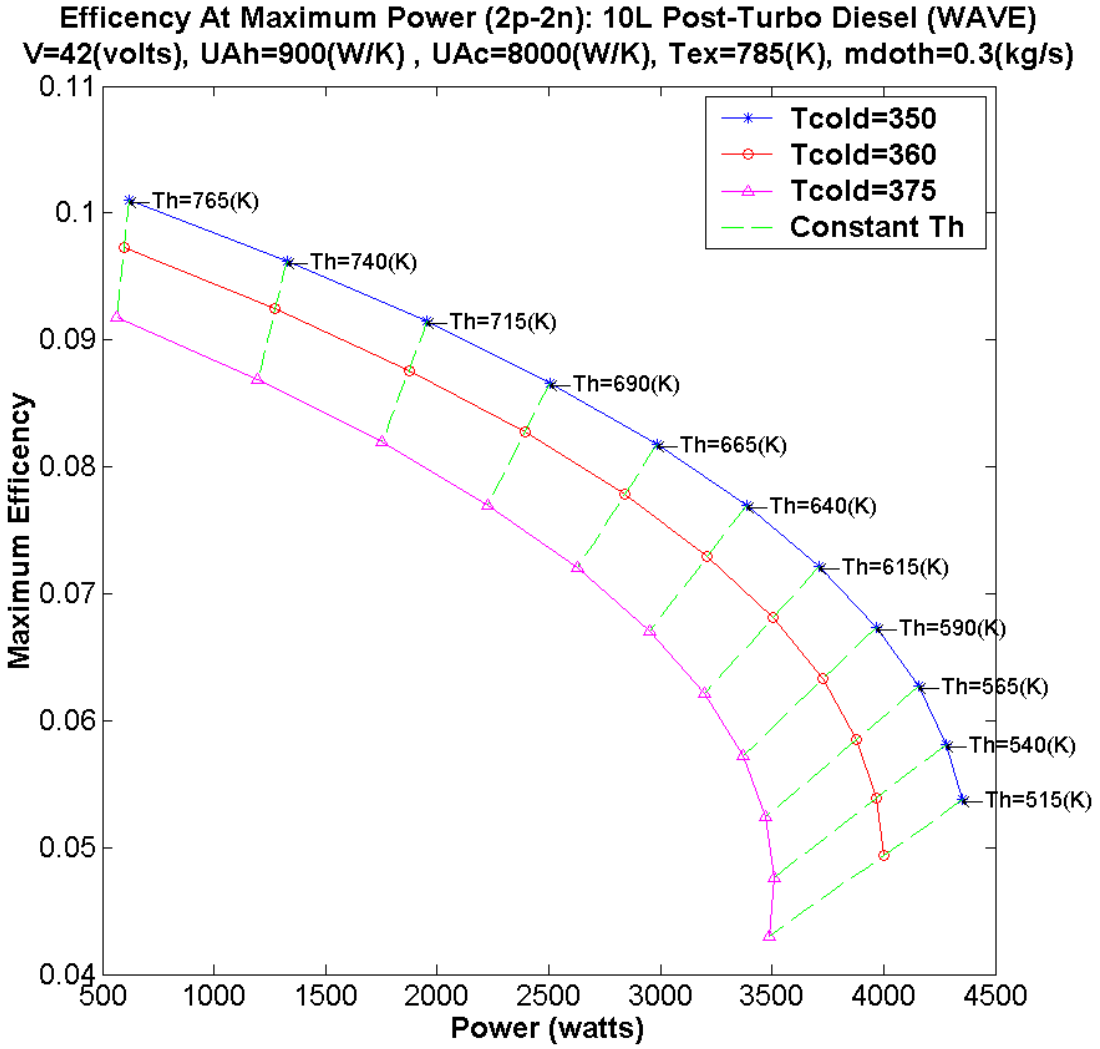

Figure 49 Efficiency vs. Maximum Electrical Power Output for Skutterudite-Bi_2Te_3 and $CoSb_3$-Bi_2Te_3 Thermoelectric Device in WAVE 10-L CI Engine

A different set of curves results from different engine thermal states. For example, industry data on a larger engine indicate a peak power potential of 13.6 kW at 8.5% efficiency.

In thermoelectric analysis, cold-side mass flow rate of air can be a limiting factor. Thus, water has been examined as an alternative medium for cold-side heat transfer. Reruns of Figure 45, Figure 46, and Figure 49 with water as the cold-side medium have been conducted. These data appear in Figure 50, Figure 51, and Figure 52.

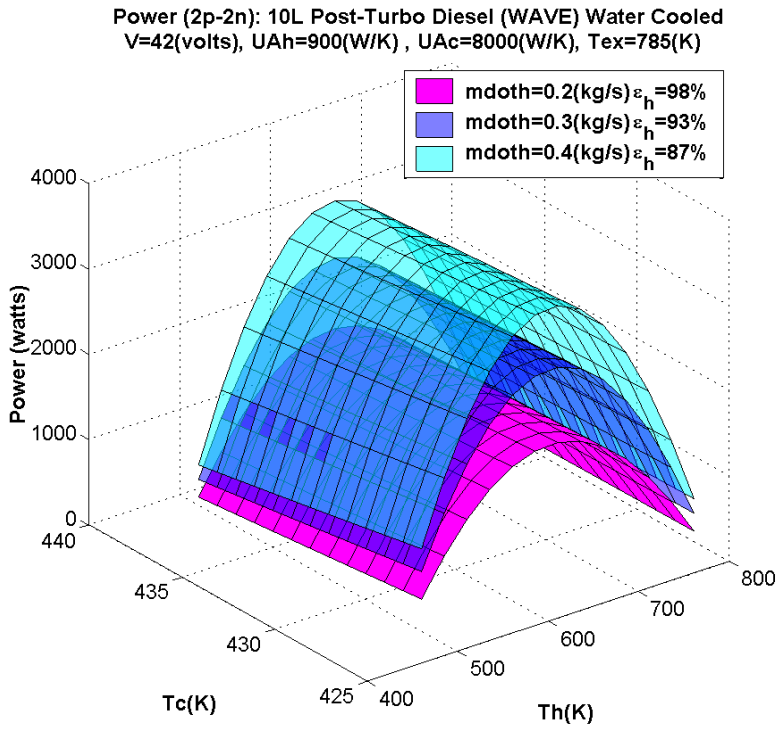

Figure 50 Predicted Electrical Power Available from TAGS-Bi_2Te_3 and 2NPbTe-Bi_2Te_3 (Hi-Z Technology Inc., San Diego, CA) Thermoelectric Material Operating at the Given Hot- and Cold-side Temperatures and Exhaust Mass Flow Rates (Water Cooled)

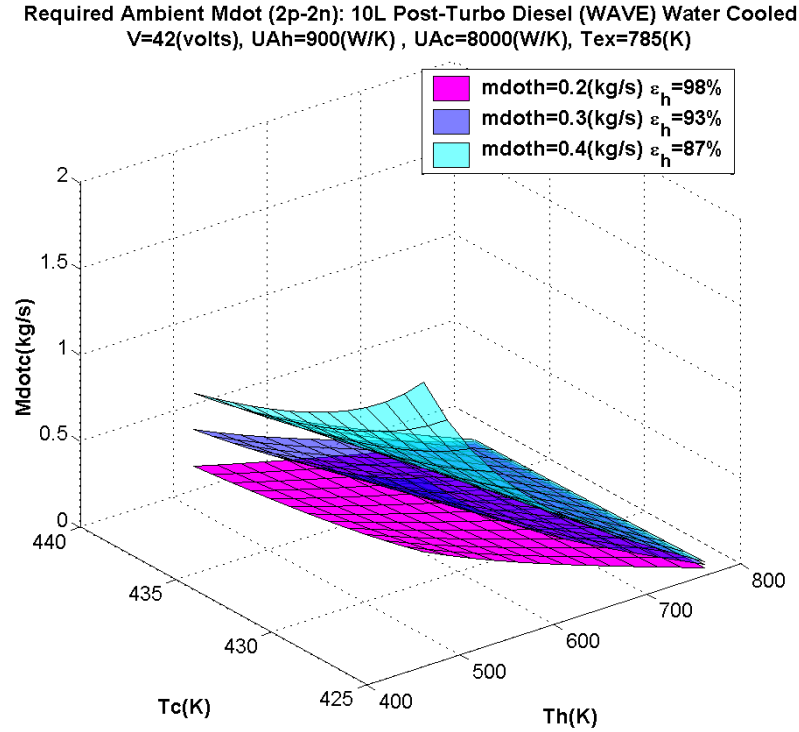

Figure 51 Required Cold-side Mass Flow Rates from TAGS-Bi_2Te_3 and 2NPbTe-Bi_2Te_3 (Hi-Z Technology Inc., San Diego, CA) Thermoelectric Material Operating at Peak Power at the Given Hot- and Cold-side Temperatures and Exhaust Mass Flow Rates (Water Cooled)

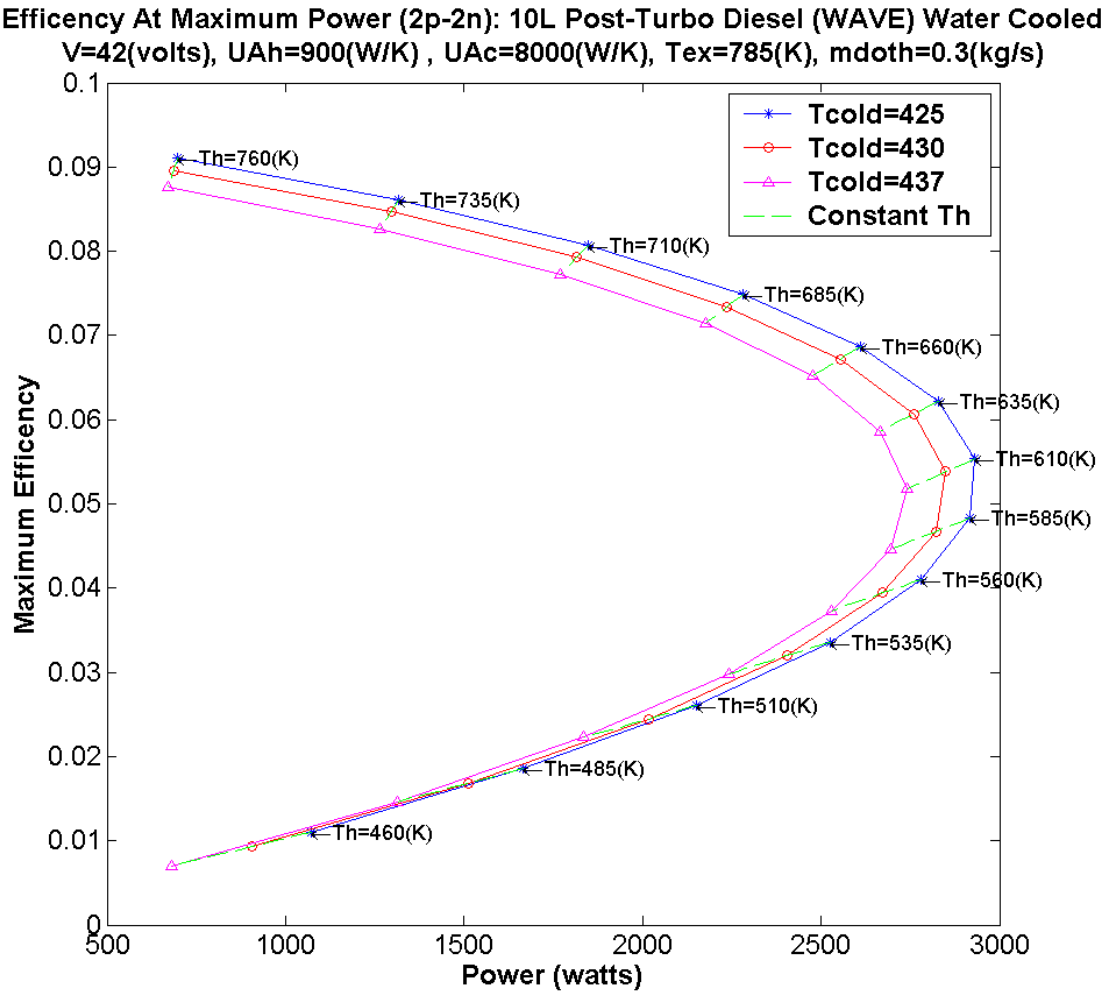

Figure 52 Efficiency vs. Maximum Electrical Power Output for TAGS-Bi_2Te_3 and 2NPbTe-Bi_2Te_3 Thermoelectric Device in WAVE 10-L CI Engine (Water Cooled)

The cold-side mass flow is much lower with water. However, the available power is diminished owing to the higher expected cold-side temperature of a closed-loop water circuit.

The analyses presented until now have dealt with thermoelectric devices positioned after the engine exhaust turbine. Another position of interest is after the engine inlet air compressor. Here, thermoelectric devices could be part of an inter-cooler; that is, the charge air can be cooled and electricity created at the same time. Studies to determine mass flow requirements and peak power by heat exchanger efficiency are shown in Figure 53 and Figure 54.

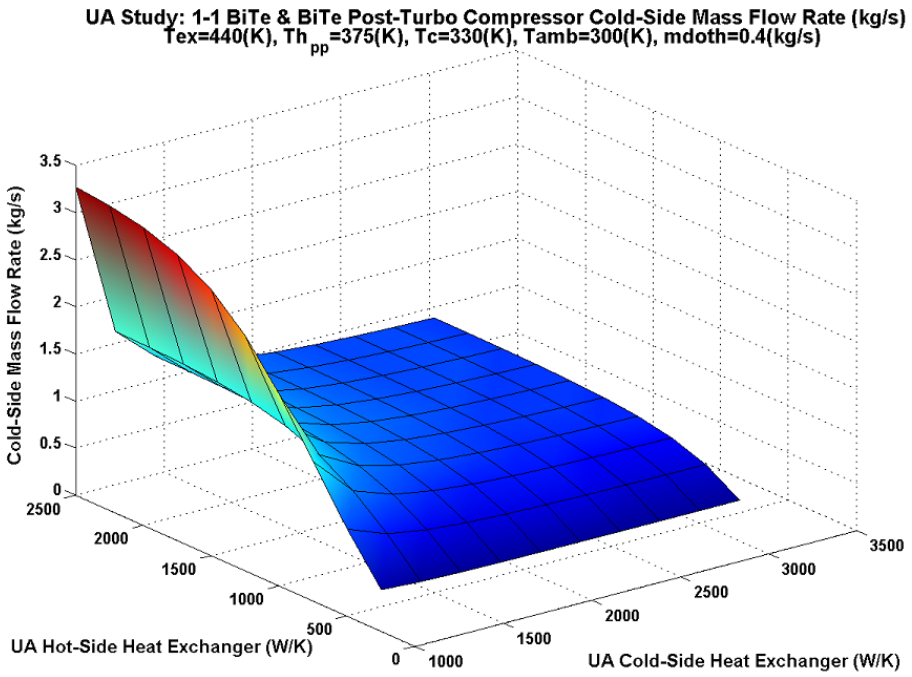

Figure 53 Cold-side Mass Flow Rate Requirements for a Post-compressor Thermoelectric Device

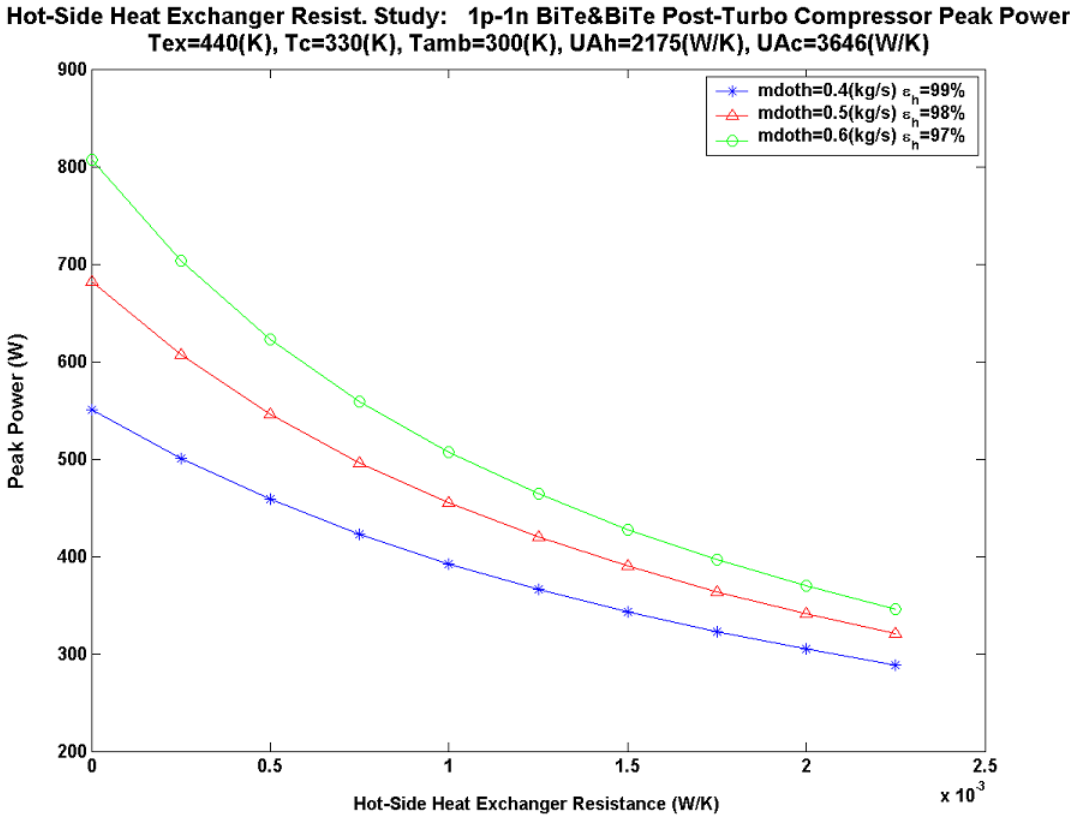

Figure 54 Peak Power by Heat Exchanger Resistance for a Post-compressor Thermoelectric Device

3.5 Vehicle Solar Load Estimator

VSOLE stands for Vehicle SOlar Loads Estimator. VSOLE was created at NREL. VSOLE, which is coded in MATLAB, calculates solar radiation transmitted, absorbed, and reflected by vehicle window glazings. This enables calculation of the solar load on a vehicle, which is important for cabin thermal modeling and human comfort (Rugh *et al.* 2001, McGuffin 2001, Farrington *et al*. 1999, Farrington *et al*. 2001).

Actual solar load depends on many factors, including glazing location and optical properties, vehicle geometry and orientation, time of day, and radiation source. The angular dependence of the optical properties for glass is also a factor. Analysis of glazing properties and comparisons of different glazings can be conducted. In addition, total solar radiation data for U.S. cities can be used with VSOLE. Thus, VSOLE makes it easy to quickly assess vehicle solar loading.

VSOLE has not yet been applied to anything larger than a sport utility vehicle or van, but it could be used to assess solar loading in larger vehicles. VSOLE is available on the Web at the same location as ADVISOR 2002 (ADVISOR 2002).

3.6 WAVE

WAVE is a one-dimensional engine performance and gas dynamics simulation software program. It comes packaged with links to several other popular simulation packages, including MATLAB/Simulink. A proof-of-concept co-simulation between MATLAB/Simulink and WAVE was run. However, WAVE may be more valuable as a stand-alone model than as part of a co-simulation.

WAVE can serve as a pre-processor for ADVISOR and other NREL system analysis tools. Engine testing is expensive and time consuming. Thus, an engine model able to run "what-if" scenarios and predict thermodynamic states is very valuable. WAVE has been used to generate efficiency maps for use in ADVISOR and to predict exhaust thermodynamic properties for NREL's thermoelectric work.

NREL recently received a validated engine model from Ricardo (the manufacturer of WAVE) through contract. The model represents the Ford Powerstroke/Navistar T444 7.3-L engine. The WAVE engine model reproduces validation test data reasonably well (Figure 55 through Figure 60—provided by Ricardo). Test data are compared with predicted values at partial load and full load.

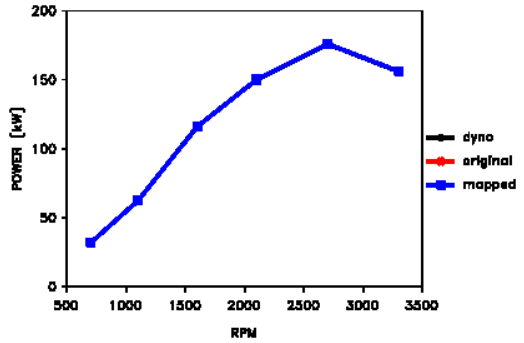

Figure 55 Full-load WAVE-mapped Engine Power vs. Tested Power

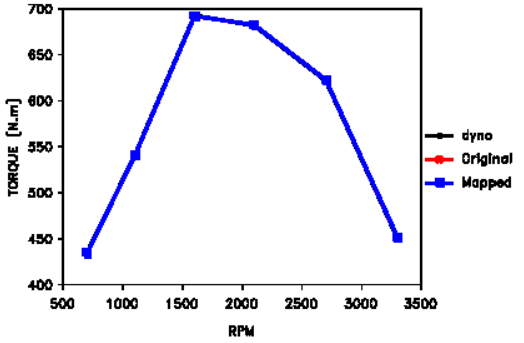

Figure 56 Full-load WAVE-mapped Engine Torque vs. Tested Torque

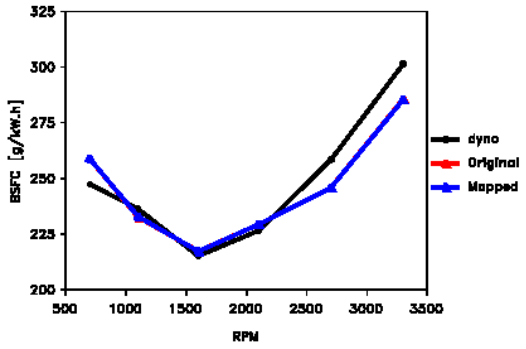

Figure 57 Full-load WAVE-mapped Engine Brake-specific Fuel Consumption (BSFC) vs. Tested BSFC

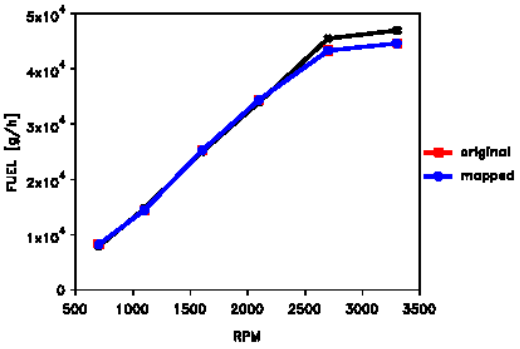

Figure 58 Full-load WAVE-mapped Engine Fuel Rate vs. Tested Fuel Rate

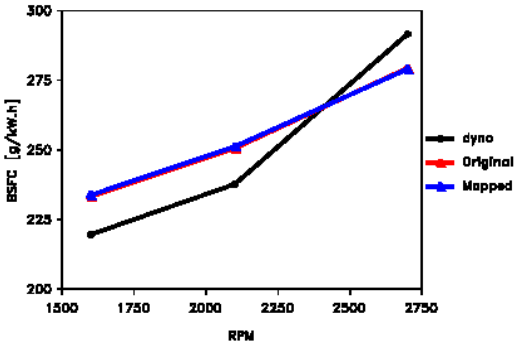

Figure 59 Partial-load WAVE-mapped Engine BSFC vs. Tested BSFC

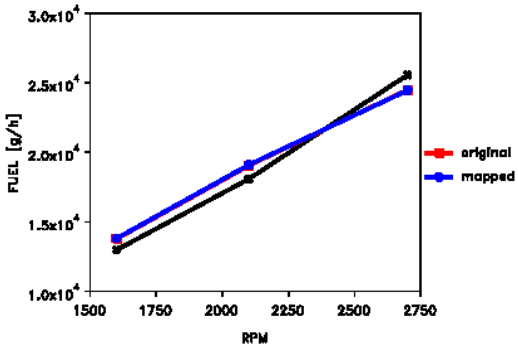

Figure 60 Partial-load WAVE-mapped Engine Fuel Rate vs. Tested Fuel Rate

An efficiency map from the Navistar T444 WAVE engine model is shown in Figure 61. The black circles give the maximum torque generated by WAVE for each speed simulated. For comparison, Figure 62 is an efficiency map created from the original test data.

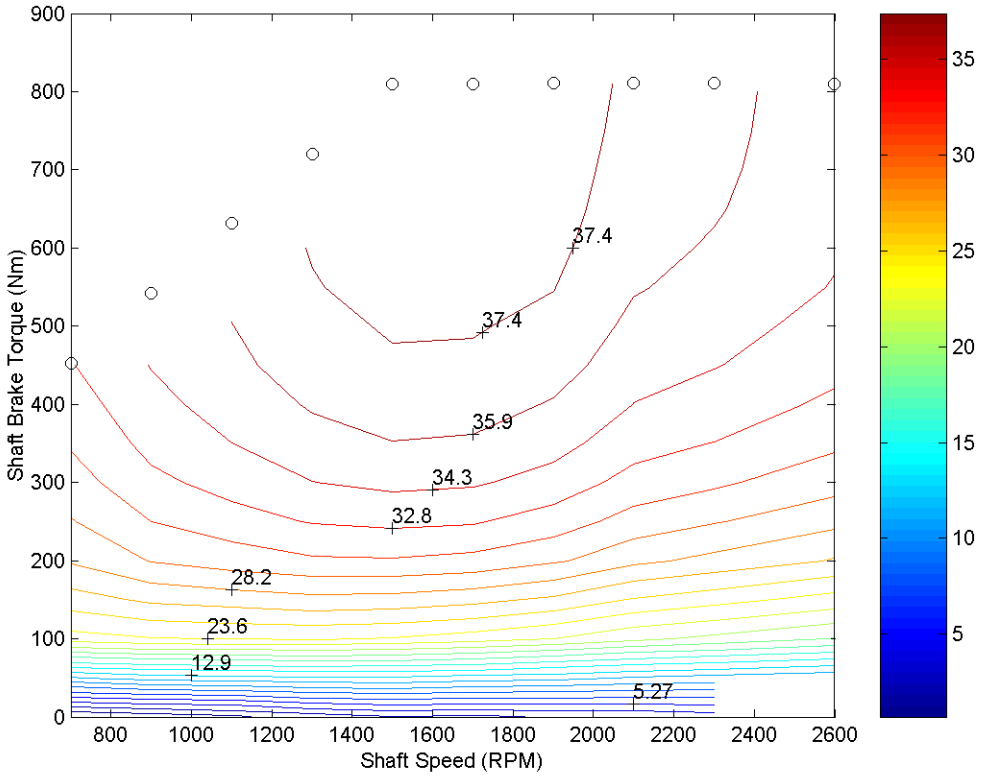

Figure 61 WAVE-generated Engine Map Showing Efficiency by Torque and Speed (Based on Navistar T444)

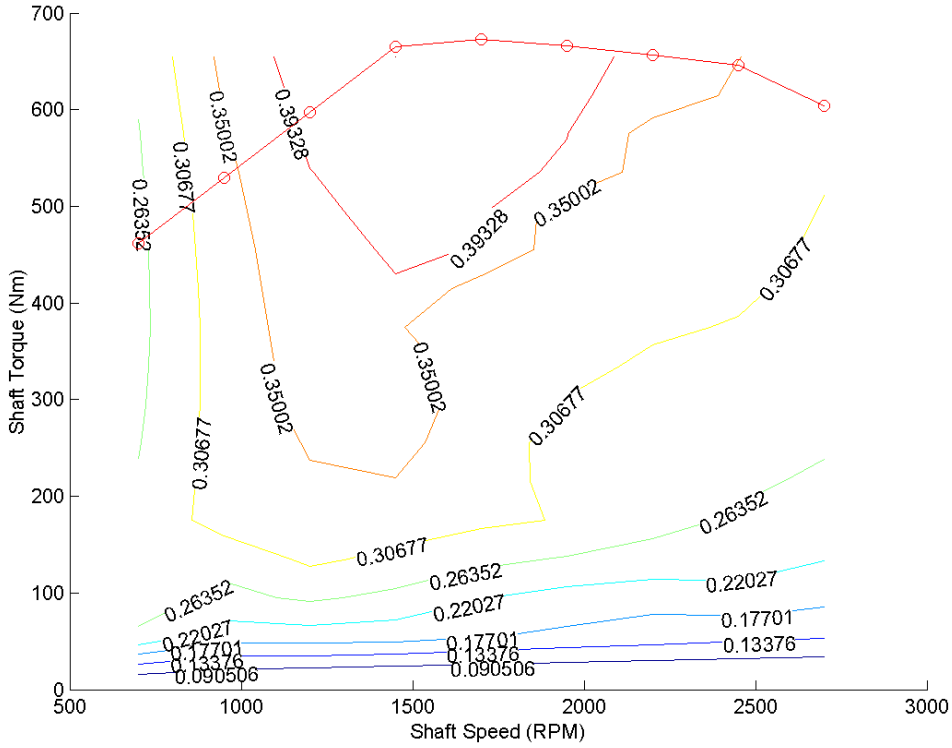

Figure 62 Efficiency Map Generated Using Base Data

The difference between the efficiency maps and maximum torque curves of Figure 61 and Figure 62 is shown in Figure 63. The jagged line for the maximum torque curve occurs because both torque curves are overlaid and points connected. The maximum torque curves differ, but efficiency (expressed as a decimal between 0 and 1) is similar. A comparison between the WAVE model and actual test data points is shown in Table 8, Appendix A.

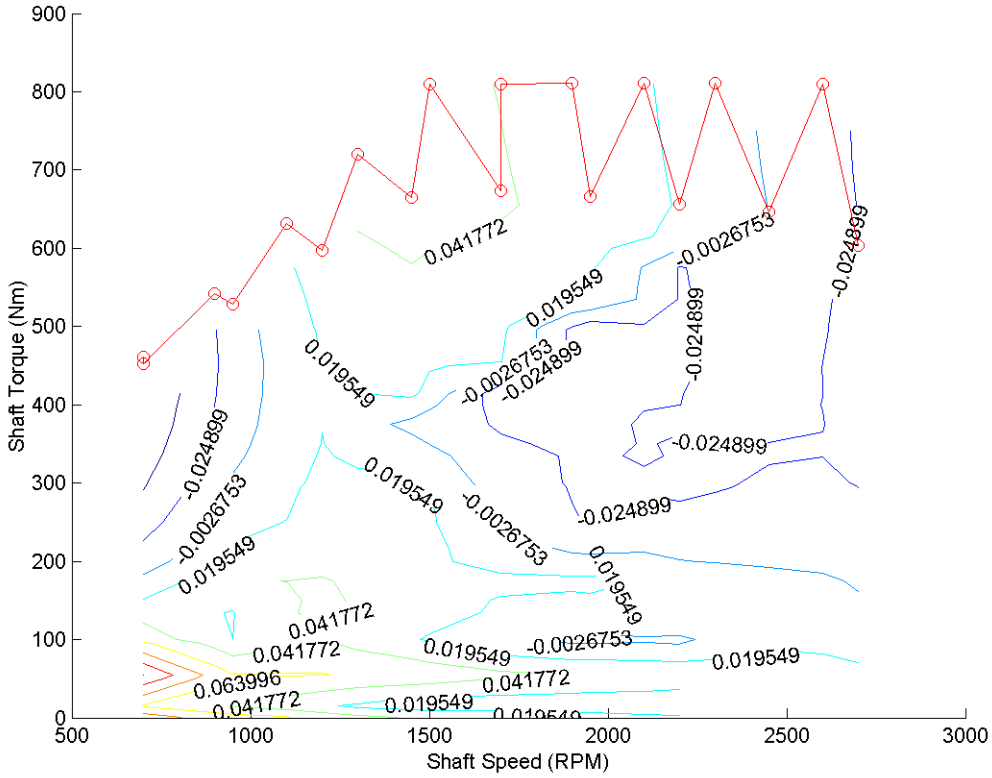

Figure 63 Difference Map Showing Difference Between WAVE-predicted Efficiency and an Engine Map Based on Test Data

As Table 8 indicates, fine tuning may be required to achieve a better match with the test data. Once the model is validated, a wealth of information is available for use in other analyses. For example, Figure 64 and Figure 65 show exhaust temperature and exhaust mass flow by engine output torque and speed. These data can be used in thermoelectric analyses (section 3.4). In Figure 64, WAVE predicts exhaust temperature to be independent of torque (i.e., loading). These and other results must be validated before work continues.

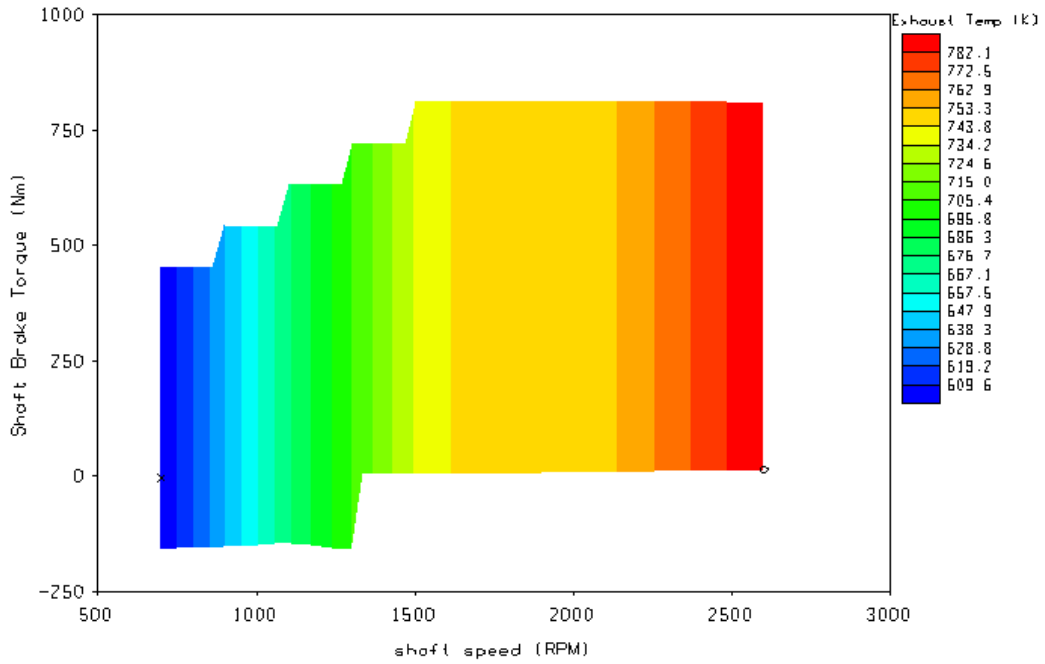

Figure 64 Engine Exhaust Temperature by Shaft Torque and Speed as Predicted by WAVE Navistar T444 Model

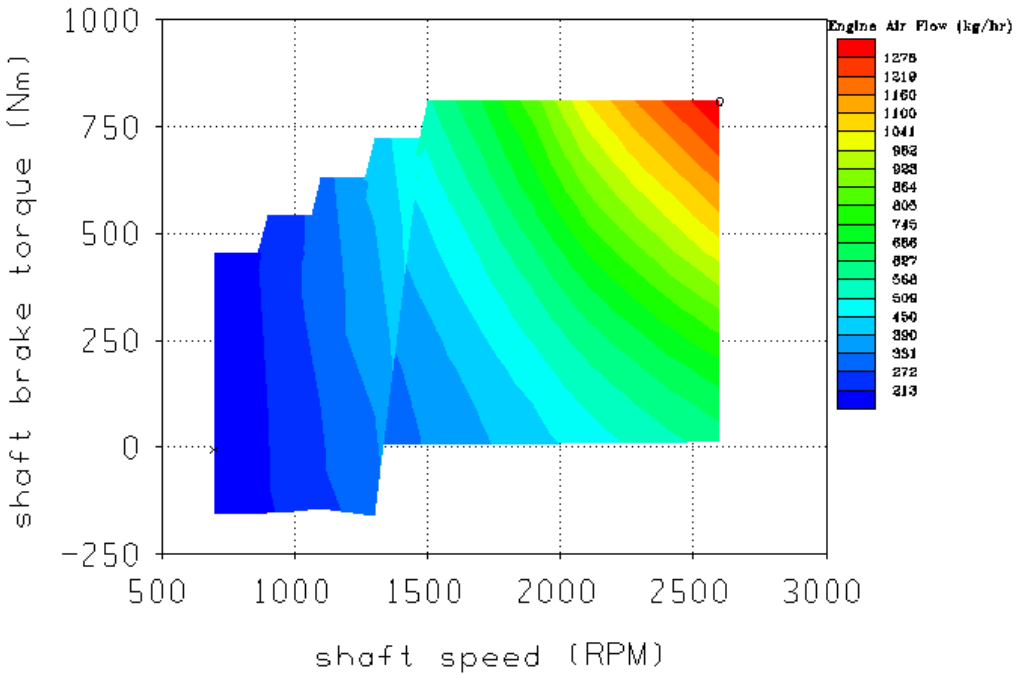

Figure 65 Engine Exhaust Mass Flow Rate as Predicted by WAVE Navistar T444 Model

4 Next Steps

4.1 ADVISOR Auxiliary Load Model

The ability to specify auxiliary loading versus time in ADVISOR would allow a user to input measured test data directly. This feature is useful and easy to implement.

In terms of application, model validation is still required. For validation, an application using real-world data on auxiliary loading and load schedules would be ideal.

These developments and applications will lend confidence to the model. In addition, this information will play a role in the DOE Essential Power System Program (EPS 2001, Virden 2002).

4.2 Saber Co-simulation

NREL is currently working on the implementation of a series and parallel drive train in Saber and ADVISOR. ADVISOR will continue to model the mechanical side of the drive train. The Saber models will include all the electrical elements (e.g., motor, generator, battery, and power electronics). This functionality will allow vendors and electronics suppliers to assess the fuel economy impacts of their designs.

4.3 SINDA/FLUINT Co-simulation Model

Validation of the current model will be a key "next step" with the SINDA/FLUINT A/C model. A secondary goal of this work is to make the co-simulation more robust and user-friendly.

Once confidence in the model has been gained, several design issues can be explored. Possible topics include A/C optimization, electrical versus mechanical A/C systems, effect of refrigerants, and use of variable displacement systems. Coupled with a sound system analysis approach, the SINDA/FLUINT A/C model will help to identify ways to reduce cabin-cooling loads.

4.4 Thermoelectric Models

There are many future applications of NREL's thermoelectric models. One possible topic is the quantification of potential waste energy recovery by thermoelectric device location on the engine manifold. Other possible applications involve waste heat recovery in fuel cells. A full transient-mode energy recovery analysis is the goal. Industry partnership with thermoelectric manufacturers will be important in bringing these devices to fruition.

4.5 VSOLE and Cabin Thermal Modeling

VSOLE is largely ready to use. New window geometries corresponding to trucks and buses can be input into VSOLE. Thus, the solar load into a cab or bus can be calculated though some manual work may be required. Applying VSOLE to trucks and buses and linking VSOLE with CFD codes for cabin thermal modeling are logical next steps.

4.6 WAVE

Work with WAVE as a pre-processor to generate critical information for ADVISOR will continue. However, an understanding of discrepancies between WAVE predictions and test data is needed to gain confidence in the model. As part of a contract with Ricardo, NREL will receive a WAVE model of a line-haul tractor-trailer engine. This model will be used with thermoelectric modeling, waste energy recovery analysis, and other applications.

5 Conclusion

NREL has begun to enhance its analytical capability to examine, quantify, and improve the energy use of vehicle auxiliary systems. Enhancements have been made to several system analysis tools, including ADVISOR. ADVISOR can simulate hybrid, fuel cell, and electric vehicles. The results of these modeling enhancements have been disseminated via technical papers and ADVISOR documentation.

Auxiliary load applications for several different models and methods are presented in this paper. These include ADVISOR auxiliary load models, model co-simulations with Saber and SINDA/FLUINT, thermoelectric models, VSOLE, and WAVE.

ADVISOR auxiliary load models offer speed-dependent mechanical and time-variable electrical load modeling. Saber co-simulation with ADVISOR enables assessment of the fuel economy impact of detailed electrical models. SINDA/FLUINT co-simulation with ADVISOR allows vehicle A/C systems and fuel economy impact to be modeled in detail.

Thermoelectric models assess the possible energy that can be recovered from waste heat. VSOLE assesses the solar loading on a vehicle, which is important for cabin thermal analysis. WAVE is an engine model capable of generating key thermal information for ADVISOR and other tools.

Several of these modeling enhancements have played key roles in completing technical analyses. Logical next steps with these models include validation and application with industry partners.

6 Bibliography

21CT 2000 — 21CT. (December 2000). "Technology Roadmap for the 21st Century Truck Program: A Government-Industry Research Partnership." Report No. 21CT-001. Available on-line, http://www.osti.gov/bridge.

ADVISOR 2002 — ADVISOR. (2002). Web site and download information, http://www.ctts.nrel.gov/analysis/.

Clark *et al.* 1999 — Clark, N.; Daley, J.; Nine, R., Atkinson, C. (1999). "Application of the New City-Suburban Heavy Vehicle Route (CSHVR) to Truck Emissions Characterization." SAE Paper No. 1999-01-1467. Warrendale, PA: SAE International.

Cullimore and Hendricks 2001 — Cullimore, B.; Hendricks, T. (2001). "Design and Transient Simulation of Vehicle Air Conditioning Systems." Prepared for the Fourth Vehicle Thermal Management Systems, London, U.K., week of May 24, 2001. SAE Paper No. 2001-01-1692. Warrendale, PA: SAE International, 10 pp.

EPS 2001 — EPS. (2001). Web site of the 2001 Essential Power System Workshop in Washington, D.C., December 12-13, 2001, http://www.trucks.doe.gov/publications/2001_EPS_Workshop.html.

Farrington *et al.* 1999 — Farrington, R.; Anderson, R.; Blake, D.; Burch, S.; Cuddy, M.; Keyser, M.; Rugh, J. (1999). "Challenges and Potential Solutions for Reducing Climate Control Loads in Conventional and Hybrid Electric Vehicles." Prepared for the VTMS4. Golden, CO: National Renewable Energy Laboratory. Available on-line, http://www.ott.doe.gov/coolcar/pubs.html.

Farrington *et al.* 2001 — Farrington, R.; Barber, G.; Hendricks, T.; Marion, W.; Markel, T.; McGuffin, R.; Rugh, J. (2001). "Integrated Modeling to Predict Occupant Thermal Comfort." Prepared for the Florence ATA 2001, 7th International Conference & Exhibition: The Role Of Experimentation In The Automotive Product Development Process, Palazzo Degli Affari, Firenze, Italy, May, 23-25, 2001. Paper No. 01A1024, 14 pp.

Hendricks 2001a — Hendricks, T. (2001). "Vehicle Transient Air Conditioning Analysis: Model Development & System Optimization Investigations." NREL/TP-540-30715. Golden, CO: National Renewable Energy Laboratory, 43 pp.

Hendricks 2001b — Hendricks, T. (2001a). "Optimization of Transient Air Conditioning Systems Using Transient Air Conditioning Performance Analysis." Prepared for the Fourth Vehicle Thermal Management Systems, London, U.K., week of May 24, 2001. SAE Paper No. 2001-01-1734. Warrendale, PA: SAE International, 10 pp.

Hendricks and O'Keefe 2002 — Hendricks, T.; O'Keefe, M. (2002). "Heavy Vehicle Auxiliary Load Electrification for the Essential Power System Program: Benefits, Tradeoffs, and Remaining Challenges." Prepared for the 2002 SAE International Truck and Bus Meeting and Exposition, Detroit, MI, November18-20, 2002.

Hnatczuk *et al.* 2000 — Hnatczuk, W.; Lasecki, M.; Bishop, J.; Goodell, J. (2000). "Parasitic Loss Reduction for 21st Century Trucks." SAE Paper No. 2000-01-3423. Warrendale, PA: SAE International.

Incropera and DeWitt 1990 — Incropera, F.; DeWitt, D. (1990). *Fundamentals of Heat and Mass Transfer*, 3rd Edition. New York, NY: John Wiley and Sons.

Johnson *et al.* 2001 — Johnson, V.; Brooker, A.; Wipke, K. (2001). "ADVISOR-Saber Co-simulation for Single-Voltage and Dual-Voltage Conventional Vehicles." A Milestone Report prepared for the U.S. Department of Energy under FWP HV11. Golden, CO: National Renewable Energy Laboratory.

LeTavec *et al.* 2000 — LeTavec, C.; Uihlein, J.; Segal, J.; Vertin, K. (2000). "EC-Diesel Technology Validation Program Interim Report." Prepared for the International Spring Fuels and Lubricants Meeting and Exposition, June 19-22, 2000. SAE Paper No. 2000-01-1854. Warrendale, PA: SAE International.

MacBain and Conover 2000 — MacBain, J.; Conover, J. (2000). "Dual Voltage Electrical System Simulations." SAE Paper No. 2000-01-3051. pp. 9-18, SAE Publication *Transitioning to 42-Volt Electrical Systems*. SAE SP-1556. Warrendale, PA: SAE International.

MacBain and Conover 2001 — MacBain, J.; Conover, J. (2001). "Co-simulation of Automotive Propulsion Systems." Prepared for EVS 18, Berlin, October 20-24, 2001.

MacBain and Conover 2001a — MacBain, J.; Conover, J. (2001a). "Simulation of Stop/Start Systems." Prepared for EVS 18, Berlin, October 20-24, 2001.

MacBain *et al.* 2001 — MacBain, J.; Conover, J.; Johnson, V. (2001). "Co-Simulation of Electrical and Propulsion Systems." SAE Paper No. 2001-01-2533. SP-1634. Prepared for the Future Vehicle Powertrain and Control Session, Future Transportation Technology Conference & Exposition, August 2001, Costa Mesa, CA.

Markel *et al.* 2002 — Markel, T.; Brooker, A.; Hendricks, T.; Johnson, V.; Kelly, K; Kramer, B.; O'Keefe, M.; Sprik, S.; Wipke, W. (2002). "ADVISOR: A System Analysis Tool for Advanced Vehicle Modeling." To be published in the *Journal of Power Sources.*

McGuffin 2001 — McGuffin, R. (2001). "Modeling of Human Thermal Comfort." Prepared for the Fourth Vehicle Thermal Management Systems, London, U.K., week of May 24, 2001. SAE Paper No. 2001-01-1739. Warrendale, PA: SAE International, 25 pp.

NASA 2001 — NASA Technology Brief. (2001). "Filled Skutterudites as Thermoelectric Materials." Report NPO-19909.Vol. 25, No. 6. Available on-line, http://www.nasatech.com/Briefs/June01/NPO19909.html. United States of America National Aeronautics and Space Administration, Jet Propulsion Laboratory.

Rugh *et al.* 2001 — Rugh, J.; Farrington, R.; Boettcher, J. (2001). "The Impact of Metal-free Solar Reflective Film on Vehicle Climate Control." SAE Paper No. 2001-01-1721. Warrendale, PA: SAE International, 7 pp.

SAE 2000 — SAE (2000). *Information Relating to Duty Cycles and Average Power Requirements of Truck and Bus Engine Accessories*. SAE Standard J1343. Warrendale, PA: SAE International.

Schmidt *et al.* 2000 — Schmidt, M.; Isermann, R.; Lenzen, B.; Hohenberg, G. (2000). "Potential of Regenerative Braking Using and Integrated Starter Alternator." SAE Paper No. 2000-01-1020. Warrendale, PA. SAE International.

Virden 2002 — Virden, J. (2002). "Essential Power Systems." Prepared for the 2002 Windsor Workshop, Windsor, Ontario, Canada, May 15, 2002.

Wipke *et al.* 1999 — Wipke, K.; Cuddy, M.; Burch, S. (1999). "ADVISOR 2.1: A User-Friendly Advanced Powertrain Simulation Using a Combined Backward/Forward Approach." *IEEE Transactions on Vehicular Technology: Special Issue on Hybrid and Electric Vehicles.* Available on-line, http://www.ctts.nrel.gov/analysis/reading_room.html.

Yao *et al.* 2001 — Yao, D.; Chen, G.; Kim, C. (2001). "Low Temperature Eutectic Bonding for In-plane Type Micro Thermoelectric Cooler." Proceedings of the 2001 ASME International Mechanical Engineering Congress and Exposition, New York, NY, November 11-16, 2001.

Appendix A

Table 1 Tractor-trailer Model Specifications (Based on 21st Century Truck Roadmap Model)

Variable	Value
Test mass	80,000 lb
C_D	0.65
RRC_0 (rolling resistance coefficient)	0.005 N/N
Frontal area	8.55 m^2
Engine map	Max power 332 kW, max efficiency 42%, max torque 1959 Nm, max speed 2100 rpm, max power at 2100 rpm and 1510 Nm
Transmission	Gear ratios: 11.706, 8.2, 6.06, 4.49, 3.32, 2.46, 1.82, 1.35, 1, 0.74

Table 2 Baseline Tractor-trailer Model in ADVISOR (80,000 lb GVW)

Baseline Tractor-trailer model	CSHVR drive cycle	WVU Interstate drive cycle	WVU Interstate with +/- 5% grade	Constant 65 mph
Fuel economy (mpg)	2.865	5.468	3.993	6.601
Fuel used (gal)	2.343	2.828	3.772	0.9847
Distance traveled (mi)	6.713	15.462	15.061	6.5
Time taken (sec)	1780	1640	1640	360
Fuel used per distance (gal/mi)	0.34900	0.18288	0.25046	0.15150
Mechanical auxiliary load (kW)	15	15	15	15

Table 3 Tractor-trailer Model with Speed-dependent Mechanical Loads in ADVISOR (80,000 lb GVW, variable SAEJ1343—local haul, 1466.9 W electrical load on alternator)

Tractor-trailer model with speed-variable loads	CSHVR drive cycle	WVU Interstate drive cycle	WVU Interstate with +/- 5% grade	Constant 65 mph
Fuel economy (mpg)	2.968	5.618	4.090	6.598
Fuel used (gal)	2.2619	2.7528	3.6879	0.9851
Distance traveled (mi)	6.71	15.46	15.08	6.5
Time taken (sec)	1780	1640	1640	360
Fuel used per distance (gal/mi)	0.33691	0.17801	0.24451	0.15156
Cycle-averaged mechanical auxiliary load (kW)	8.762	10.068	10.033	15.025

Table 4 Baseline Constant Electrical/Mechanical Auxiliary Load Tractor-trailer Model in ADVISOR—60% efficient alternator (80,000 lb GVW)

Baseline tractor-trailer model	CSHVR drive cycle	WVU Interstate drive cycle	Constant 65 mph
Fuel economy (mpg)	2.999	5.683	6.8459
Fuel used (gal)	2.2392	2.7221	0.94947
Distance traveled (mi)	6.7145	15.4693	6.5

Time taken (sec)	1780	1640	360
Fuel used per distance (gal/mi)	0.3335	0.17597	0.14607
Auxiliary load (kW)	7.457 kW mech. plus 0.7 kW elec. on 60% efficient alternator 8.6236 kW	7.457 kW mech. plus 0.7 kW elec. on 60% efficient alternator 8.6236 kW	7.457 kW mech. plus 0.7 kW elec. on 60% efficient alternator 8.6236 kW

Table 5 Time-variable Electrical Loads for Tractor-trailer Model in ADVISOR (80,000 lb GVW)—60% efficient alternator

Time-variable electrical loads tractor-trailer model	**CSHVR drive cycle**	**WVU Interstate drive cycle**	**Constant 65 mph**
Fuel economy (mpg)	2.99918	5.683	6.8455
Fuel used (gal)	2.23878	2.72196	0.949535
Distance traveled (mi)	6.71451	15.46939	6.5
Time taken (sec)	1780	1640	360
Fuel used per distance (gal/mi)	0.33342	0.17596	0.14608
Auxiliary load (kW)	8.6274	8.6257	8.6364

Table 6 Time-variable Electrical Loads for Tractor-trailer Model in ADVISOR (80,000 lb GVW)—Variable Efficiency Alternator with Time-variable Electrical Loads and Fixed Constant Electrical Loads

Time-variable electrical loads tractor-trailer model	**CSHVR drive cycle** **Constant 0.7 kW electrical load**	**WVU Interstate drive cycle** **Constant 0.7 kW electrical load**	**CSHVR drive cycle** **Variable 0.7 kW electrical load**	**WVU Interstate drive cycle** **Variable 0.7 kW electrical load**
Fuel economy (mpg)	3.000	5.6858	3.000	5.6857
Fuel used (gal)	2.2379	2.7207	2.2378	2.72078
Distance traveled (mi)	6.7145	15.4694	6.7145	15.4695
Time taken (sec)	1780	1640	1780	1640
Fuel used per distance (gal/mi)	0.33330	0.17588	0.33328	0.17588
Auxiliary load (kW)	8.5331	8.5377	8.5516	8.5504

Table 7 Saber Co-simulation with Tractor-trailer Model in ADVISOR (80,000 lb GVW)

Time-variable electrical loads—tractor-trailer model	**CSHVR drive cycle** **Constant 0.7 kW electrical load**
Fuel economy (mpg)	2.994
Fuel used (gal)	2.24293
Distance traveled (mi)	6.71442
Time taken (sec)	1780
Fuel used per distance (gal/mi)	0.3340462
Auxiliary load (kW)	8.8491

Table 8 WAVE-predicted Efficiency vs. 13-mode OICA* Cycle Test Data

Test data				WAVE	Difference	
Shaft speed (RPM)	**Shaft torque (Nm)**	**Brake Power (kW)**	**Test brake efficiency**	**Predicted brake efficiency**	**Delta**	**Percent difference**
700	19.3	1.4	11.4%	3.7%	7.8%	-67.9%
1350	57.4	8.1	20.8%	14.5%	6.3%	-30.3%
1100	202.4	23.3	34.4%	30.6%	3.9%	-11.2%
1600	202.4	33.9	34.2%	31.1%	3.2%	-9.3%
1350	348.5	49.3	37.8%	35.4%	2.4%	-6.5%
2480	651.6	169.2	34.7%	35.3%	-0.6%	1.6%
2600	359.6	97.9	29.7%	31.8%	-2.1%	7.2%
2700	115.4	32.6	20.8%	NA	NA	NA

*Note: OICA is the Organisation Internationale des Constructeurs d'Automobiles. The 13-mode test is used in Europe to certify heavy-duty engines.